GRADUATE AERONAUTICAL LABORATORIES

CALIFORNIA INSTITUTE OF TECHNOLOGY

GALCIT Report FM 94-2

INTERACTION OF CHEMISTRY, TURBULENCE, AND SHOCK WAVES IN HYPERVELOCITY FLOW

G. V. Candler*, P. E. Dimotakis, H. G. Hornung, A. Leonard,
D. I. Meiron, B. V. McKoy, D. I. Pullin and B. Sturtevant

*University of Minnesota

Annual Technical Report

Approved for public release; distribution is unlimited

Prepared for

AIR FORCE OFFICE OF SCIENTIFIC RESEARCH

110 Duncan Avenue, Suite B115, Bolling AFB DC 20332-0001

Firestone Flight Sciences Laboratory

Guggenheim Aeronautical Laboratory

Karman Laboratory of Fluid Mechanics and Jet Propulsion

Pasadena

DISCLAIMER NOTICE

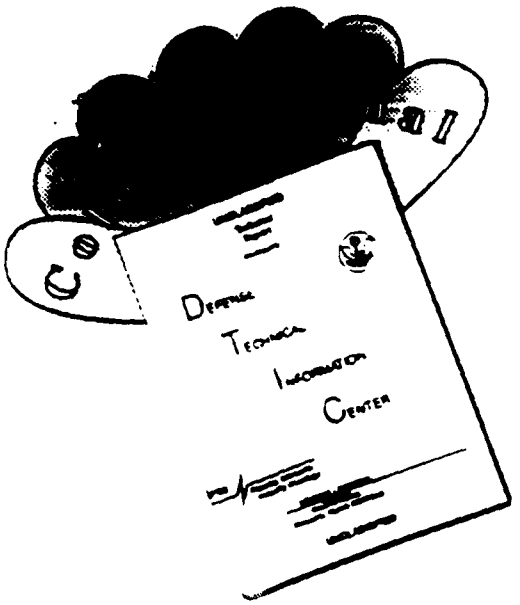

THIS DOCUMENT IS BEST QUALITY AVAILABLE. THE COPY FURNISHED TO DTIC CONTAINED A SIGNIFICANT NUMBER OF COLOR PAGES WHICH DO NOT REPRODUCE LEGIBLY ON BLACK AND WHITE MICROFICHE.

REPORT DOCUMENTATION PAGE

Form Approved
OMB No. 0704-0188

1. AGENCY USE ONLY (Leave blank)	2. REPORT DATE	3. REPORT TYPE AND DATES COVERED
	May, 1994	Ann. Tech. Rept. 5/15/93 - 5/14/94

4. TITLE AND SUBTITLE
Interaction of chemistry, turbulence, and shock waves in hypervelocity flow

5. FUNDING NUMBERS
PE - 61103D
PR - 3484
SA - AS
G - F49620-93-1-0338

6. AUTHOR(S)
G. Candler, P. Dimotakis, H. Hornung, A. Leonard, D. Meiron, B. V. McKoy, D. Pullin and B. Sturtevant
(Compiled by H. Hornung)

7. PERFORMING ORGANIZATION NAME(S) AND ADDRESS(ES)
California Institute of Technology
1201 E. California Blvd.
Pasadena, CA 91125

8. PERFORMING ORGANIZATION REPORT NUMBER
GALCIT FM 94-2
AFOSR-TR- 94 0448

9. SPONSORING/MONITORING AGENCY NAME(S) AND ADDRESS(ES)
AFOSR/NA
110 Duncan Avenue, Suite B115
Bolling AFB DC 20332-0001

10. SPONSORING/MONITORING AGENCY REPORT NUMBER

11. SUPPLEMENTARY NOTES

12a. DISTRIBUTION/AVAILABILITY STATEMENT
Approved for public release; distribution is unlimited

12b. DISTRIBUTION CODE

13. ABSTRACT (Maximum 200 words)

Significant progress was made during the first year of an interdisciplinary experimental, numerical and theoretical program to extend the state of knowledge and understanding of the effects of chemical reactions in hypervelocity flows. The program addressed the key problems in aerothermochemistry that arise from interactions between the three strongly nonlinear effects: Compressibility; vorticity; and chemistry. Important new results included:

- Experimental data on the effect of enthalpy on transition in hypervelocity flow. First visualization of high-enthalpy turbulent boundary layer structure.
- New data on hypervelocity flow over spheres, confirming computations and new theory.
- Progress on methods of parallel computation of shock-vortex interaction. New computations of three-dimensional leeward reacting flow.
- Development and tests of a greatly improved low-cost thermocouple heat transfer gauge.
- Upgrade of the supersonic shear-layer facility to all-hyperbolic operation. Exploration of this regime with a new Rayleigh scattering method.
- Test of the validity of vibration-dissociation coupling models from shock tunnel data.
- Successful application of new parallelized algorithm of the extended Schwinger multi-channel method to computation of electron-molecule collision cross-sections.
- Prediction and realization of a new non-intrusive diagnostic method, laser-induced thermal acoustics, for accurate measurement of sound speed and bulk viscosity.

14. SUBJECT TERMS	15. NUMBER OF PAGES
chemical reaction, shock wave, vorticity, hypervelocity, shock-vortex interaction, heat transfer gauges, laser scattering, laser-induced thermal acoustics, vibration-dissociation coupling	64
	16. PRICE CODE

17. SECURITY CLASSIFICATION OF REPORT	18. SECURITY CLASSIFICATION OF THIS PAGE	19. SECURITY CLASSIFICATION OF ABSTRACT	20. LIMITATION OF ABSTRACT
Unclassified	Unclassified	Unclassified	UL

GALCIT Report FM 94-2

INTERACTION OF CHEMISTRY, TURBULENCE AND SHOCK WAVES IN HYPERVELOCITY FLOW

G. V. Candler*, P. E. Dimotakis, H. G. Hornung, A. Leonard,
D. I. Meiron, B. V. McKoy, D. I. Pullin and B. Sturtevant

California Institute of Technology
Pasadena, CA 91125
*University of Minnesota

17 May 1994

Annual Technical Report

Approved for public release; distribution is unlimited

Prepared for

AIR FORCE OFFICE OF SCIENTIFIC RESEARCH

110 Duncan Avenue, Suite B115, Bolling AFB DC 20332-0001

EXECUTIVE SUMMARY

We report on the technical progress in the first year of an interdisciplinary experimental, numerical and theoretical program to extend the state of knowledge and understanding of the effects of chemical reactions in hypervelocity flows. The program combines unique experimental and computational facilities at Caltech to address the key problems in aerothermochemistry that arise from interactions between the three strongly nonlinear effects: Compressibility; vorticity; and chemistry. Fig. 1 presents an overview of the program.

Project / Investigator	I.1. Hornung	I.2. Hornung	I.3. Sturtevant	II.1. Wilkinson, Pullin	II.2. Sturtevant	III. Dimotakis	IV.1. Candler	IV.2. Mckay	IV.3. Pullin	V.2. Hornung
I.1. Transitional and Turbulent Boundary Layers		●	●		●	●	●			●
I.2. Nonequilibrium and Vorticity Downstream of Bow Shocks	●		●	●			●		●	●
I.3. Ablation With Chemical Reaction	●	●		●	●			●		●
II.1. Nonequilibrium Chemistry in Shock–Vortex Interaction		●	●		●	●	●	●	●	
II.2. Shock Wave Interactions in Hypervelocity Flow	●		●	●			●		●	●
III. Supersonic Shear–Layer Flows	●			●						●
IV.1. Measurement of Vibrational Nonequilibrium Reaction Rate	●	●		●	●			●	●	●
IV.2. Rates of Electron Driven Reactions in Hypersonic Flow			●	●			●		●	
IV.3. Nonequilibrium Leeward Shock–Vortex Aerodynamics		●		●	●		●	●		
V.2. DFWM for Composition and Temperature Measurement	●	●	●		●	●	●			

Fig. 1. Sub-projects, principal investigators, and main interactions.

The program has led to the following important new results (partial list):

- Extensive experimental data on the effect of enthalpy on transition in hypervelocity flow. First visualization of high-enthalpy turbulent boundary layer structure.
- Extensive new data on hypervelocity flow over spheres, confirming numerical and new theoretical results as well as T5 enthalpy.
- Progress on methods of parallel computation of shock-vortex interaction. New computations of 3-D leeward reacting flow.
- Development and tests of a greatly improved low-cost thermocouple heat transfer gauge.
- Upgrade of the supersonic shear-layer facility to all-hyperbolic operation. Experimental exploration of this regime with a new Rayleigh scattering method.
- Test of the validity of vibration-dissociation coupling models from T5 data and computation.
- Successful application of new parallelized algorithm of the extended Schwinger multi-channel method to computation of electron-molecule collision cross-sections.
- Prediction and realization of a new non-intrusive diagnostic method, laser-induced thermal acoustics (LITA), for accurate measurement of sound speed and bulk viscosity.

The research has benefited extensively from close interaction within the program, including regular research conferences and seminars, and through extensive communication with outside groups through presentations at conferences and seminars, as well as through consultancies. In most of the sub-projects the progress made at least measured up to our initial plans, and in some cases went well beyond, through favorable developments during the year. The research has led to 3 Ph.D. degrees and produced 14 publications. The sub-projects are actively producing results at present.

TABLE OF CONTENTS

INTRODUCTION

Background

At the outset of this report it is pertinent to quote three of the opening paragraphs of the proposal that led to the current URI Grant:

"Transport to or from space, aero-assisted orbital transfer operations and other hypervelocity flight maneuvers necessarily occur at such high (near orbital) speeds, that the bow-shock heating of the components of air causes them to be dissociated, to react with each other, and, at particularly high speeds, to be ionized. Efficient air-breathing propulsion of such high-speed vehicles also requires supersonic combustion of the fuel. To a large degree, these applications have motivated the interest in the field of study that has been named aerothermochemistry by von Karman.

The character of the dynamics of reacting gases is changed relative to perfect-gas dynamics in two important ways: First, the equilibrium behavior is much more complicated, and second, characteristic times are introduced by the fact that the reactions proceed at finite rates. These two types of highly nonlinear gas imperfections, interacting with the classical nonlinear manifestations of gas-dynamics, namely shock waves and turbulence, produce many new flow structures and phenomena. Some of these are known and qualitatively understood, a few are quantitatively predictable by computation, all are of scientific, and most of practical importance to the operations listed above. The experimental data in this field are very limited, because of the difficulties associated with laboratory simulation. This constitutes the most important need in aerothermochemistry.

The proposed research work may be grouped under the following major headings:

supersonic turbulent mixing and combustion
effects of chemical reactions in external hypervelocity flows
reaction rate models

The philosophy of this proposal is to concentrate interdisciplinary effort on particular problems in the first two categories. The main thrust of the proposed research is to use the two new facilities (T5 hypervelocity shock tunnel and S^3LSupersonic Shear-Layer Facility) for an experimental program to study and understand the effects introduced by chemical reactions. A parallel theoretical and computational effort will help design the experiments and test models and mechanisms of the gas behavior. The third category pervades the whole program and represents research in theoretical and computational chemistry and fluid dynamics, as well as comparison with experiment."

The program was then subdivided into the following four parts

I. Reaction-rate controlled shear flows
II. Shock-vorticity interactions
III Supersonic mixing and combustion
IV Chemistry in non-uniform flow,

all of which involve complicated and non-linear interaction between *vorticity, chemistry* and *compressibility.* By focusing the available facilities and expertise on the main problems in the field, sub-projects were determined as shown in Fig. refxint together with the PI's and the main interactions between them.

A brief outline of the objectives was then formulated in the following statement of work. The numbering of these sub-projects corresponds to that of the sections in this report under which the progress is described in more detail.

Statement of Work

I.1 Obtain qualitative information on the structure of transitional and turbulent boundary layers at high enthalpy. Determine the response of a laminar boundary layer to disturbances at the most strongly amplified frequency for the second mode instability. Perform T5 experiments on a sharp slender cone, using differential interferometry, laser-induced fluorescence and surface instruments.

I.2 Design experiments for testing the limits of binary scaling by making a numerical study of blunt body flows in nitrogen and air. Carry out T5 experiments on spheres using surface instrumentation, differential interferometry and degenerate four-wave mixing (DFWM). Extend the experiments to study the high-vorticity layer downstream of a bow shock associated with the large density rise caused by dissociation.

I.3 Determine the flux of reactive and inert species, and of heat and momentum to the surface of ablating bodies in hypervelocity flow. Carry out T5 experiments using sampling mass-spectrometric analysis and surface heat transfer and pressure measurements. Formulate analytical models of reactive effects on ablation.

II.1 Perform ultra-high resolution numerical experiments combined with nonlinear analysis and numerics to establish appropriate initial conditions to elucidate the generic mechanisms of shock-vortex interactions, namely, (1) interaction of a shock with a vorticity field in the presence of nonequilibrium chemistry, and (2) vorticity generation in shock focusing with chemistry.

II.2 Determine the effects of chemical relaxation on the shock-on-shock problem. Demonstrate the magnitude of nonequilibrium effects on shock impingement heating. Carry out experiments with a 2-dimensional model in T5, supported by local shock-polar analysis and numerical calculations of an ideal dissociating gas.

III Carry out S^3L experiments with chemically reacting and non-reacting flows, using schlieren, spectroscopy, Rayleigh scattering, chemical effects and new diagnostic methods, to gain understanding of the mechanisms of mixing when a shock interacts with a supersonic turbulent shear layer, and in the flow downstream of an expansion wave. Develop new related diagnostics and computational capabilities.

IV.1 Design and carry out an experiment in T5 to provide data to test chemical reaction models for flows with vibrational nonequilibrium. Use a previously developed computational technique to simulate the flow over proposed experimental configurations. Identify a configuration that exhibits significant effects of vibrational nonequilibrium on the reaction rates.

IV.2 Exploit computational methodologies and high-performance and cost-effective computing provided by highly parallel and scalable supercomputers to solve the complex equations which govern electron-molecule collision processes needed for robust modeling of the chemical and physical properties of hypervelocity flows.

IV.3 Demonstrate the effect of chemistry on the leeward shock-vortex separation region of hyper-

velocity flow about slender bodies using high-resolution CFD on the Intel Touchstone-Delta computer, combined with dimensional analysis and physical scaling.

V.2 Develop DFWM for measuring species concentration and temperature in hypervelocity flows. concentrate on NO-concentrations because of their importance in air flows. Buy the remaining equipment to complete the set of components, assemble the instrumentation, debug and apply it to T5 flows.

Current Status of Progress

In the following paragraphs, which mirror the statement of work, the progress in the subprojects is summarized.

I.1 Extensive experiments were conducted over the enthalpy range $3.5\,\mathrm{MJ/kg} < h_0 < 22\mathrm{MJ/kg}$ in air and nitrogen, and $3.5\,\mathrm{MJ/kg} < h_0 < 8.6\mathrm{MJ/kg}$ in carbon dioxide, with laminar, transitional and turbulent flow on a slender cone. Flow visualization with a novel method and heat flux measurements show that the mechanism of transition under the conditions examined is via the Tollmien-Schlichting instability. High-enthalpy real-gas effects have a strongly stabilizing effect, which appears to scale with total enthalpy normalized by dissociation energy.

I.2 A series of experiments on flow over spheres has been completed that covers the full range of enthalpy of T5 in air, nitrogen and CO_2 using interferometry and heat flux measurements. Numerically computed interferograms agred well with experiment except in small regions near the shock (see also IV.1). Theoretical analysis of the problem led to a complete understanding of the correlation of the dimensionless stand-off distance with dimensionless reaction-rate parameter, and its extension to reacting gas mixtures. A previous theoretical analysis of dissociating flow along a streamline downstream of a curved shock has been extended to include the effects of recombination. The limits of binary scaling were delineated. Initial exploratory experiments on the detection of the high vorticity layer and its stability were performed.

I.3 This subproject is not scheduled to start until the end of the second year, when it is planned that it will follow the completion of the work under II.2. preliminary plans for the mass-spectrometer design have been made but are not reported in detail.

II.1 Progress has been made in computation of steady compressible vortex structures which will then be used as special initial conditions for controlled numerical experiments on shock vorticity interaction. Progress has also been made in developing the computational capability for simulation of vorticity generation through shock focusing. A large scale two dimensional compressible flow solver has been constructed and a high resolution study has been started on two massively parallel machines including the Intel Delta and the IBM SP/1. Whitham theory was applied to the computation of an approximation for the vorticity generated by a shock as it interacts with a density gradient. Computations are now in progress to test this approximation.

II.2 The primary effort during this reporting period was to make major improvements in methods for heat transfer measurement and optical interferometry in T5. In addressing the planned improvement of the existing Wollaston prism differential interferometer, a more sweeping solution was sought; a completely new holographic system for optical diagnostics in T5 has been designed and built. This instrument will be reported at another time. In this report we doc-

ument the development of a new heat transfer gauge which gives performance superior to any existing device.

III In the compressible shear-layer turbulence and supersonic mixing part of this effort we have upgraded the supersonic shear layer (S^3L) facility to accommodate bi-supersonic flow, *i.e.*, both freestreams supersonic, resulting in an all-hyperbolic flow configuration. A first set of experiments were performed in this flow regime. A second generation, higher signal-to-noise ratio, planar, laser Rayleigh-scattering experiments were performed in supersonic shear layers with varying degrees of compressibility, which indicate the existence of a high-compressibility flow regime with different entrainment and mixing mechanisms. Computationally, we have performed simulations of bi-supersonic and transonic shear-layer flows that reproduce many of the features observed in our preliminary experiments in this flow regime.

IV.1 All currently-used vibration-dissociation coupling models have been implemented in a two-dimensional thermo-chemical nonequilibrium computational fluid dynamics method. The flow of reacting nitrogen over a sphere has been simulated using these models and compared to available experimental data from T5. Under the conditions of the flow tested, it was found that while the various models gave different vibrational temperature distributions, the shock stand-off distances and density contours are very similar. A new experiment is being designed for T5 that will be more sensitive to the differences in the reaction rate models. Simulations have been made of T 5 flows over spheres at lower densities, and differences among the models are discernible in both the shock stand-off distances and the density contours.

IV.2 The computationally most intense step of the previously developed program for computation of low-energy electron-molecule collisions with the extended Schwinger multi-channel method has been parallelized. Sustained performance has been achieved at about 4 GFLOP on the full Intel Delta, approximately 100 times the performance of the original sequential program on the CRAY Y-MP. The program has been used in the computation of a number of important collision processes and cross-sections.

V.2 In this sub-project, a new diagnostic method, laser-induced thermal acoustics (LITA), was discovered which is more powerful than the originally planned DFWM. The theory of LITA was developed, and this predicted that the technique would permit non-intrusive measurement of the speed of sound and the bulk viscosity of a gas. Extensive equipment was bought and the method was developed and tested. The technique proved to be entirely successful and very accurate, with many advantages over other laser diagnostic techniques, and extensive further possibilities. The theory, developed six months before the tests, precisely predicted the recorded signals in the tests.

A total of 4 higher degrees were earned. 3 papers were published or accepted for publication in the archival literature, and 5 have been submitted or are in preparation. 10 papers were published as conference papers or in proceedings. The work has resulted in a large number of presentations at various seminars, meetings and conferences. Details of these are given in the subsections.

Interactions

The interaction between the principal investigators and their research groups within the project followed the diagram in Fig. 1. very closely. Much of this interaction is forced by joint use of facilities or instrumentation, sharing of technical personnel, or through discussions that arise at

almost weekly interactions in the Fluid Mechanics Research Conference at GALCIT. Interaction between the separate Aerothermodynamics URI's benefited from the meeting held at Caltech in July 1993. Advantage was taken by several PI's of attendance at conferences (AIAA, 19thISSW) and meetings at AEDC to interact with other groups nationally and internationally.

Layout

The following chapters present the main results of the work in more detail, in the order shown above. Each subproject then lists the personnel, publications, degrees earned, and interactions separately. A few of the subprojects had received preliminary funding before the URI funding began, so that they are at a more mature stage than others.

CHAPTER I

REACTION-RATE CONTROLLED SHEAR FLOW

I.1 TRANSITIONAL AND TURBULENT BOUNDARY LAYERS

Objectives and Status of Research

The objective of this experimental investigation is to obtain qualitative information on the structure of transitional and turbulent boundary layers at high enthalpy, and to determine the response of the laminar boundary layer to disturbances at the most strongly amplified frequency for the second mode instability. The experiments use surface heat transfer measurements on a slender, sharp cone and optical flow visualization to detect effects of chemical reactions on the heat transfer, transition location, and structure of the flow field. A gas-dynamical oscillator is to be used to generate the controlled disturbances.

The proposal for this sub-project of the grant was written on the basis of preliminary experiments performed with the slender cone in T5 that were reported in Ref. 1. During the reporting period an extensive investigation covered the enthalpy range $3.5\,\mathrm{MJ/kg} < h_0 < 22\mathrm{MJ/kg}$ in air and nitrogen, and $3.5\,\mathrm{MJ/kg} < h_0 < 8.6\mathrm{MJ/kg}$ in carbon dioxide. The results include extensive data on surface heat transfer on the slender cone in laminar, transitional and turbulent boundary layers, from the perfect-gas to the high-enthalpy regime, in the latter with and without recombination at the wall. A novel method is employed to visualize the boundary layer flow structure, yielding the first pictures of turbulent boundary layer structure in high-enthalpy flow. The results demonstrate that the similarity theories predict the heat transfer rate correctly in the laminar boundary layer. The mechanism of transition under the conditions examined is via the Tollmien-Schlichting instability. High-enthalpy real-gas effects have a strongly stabilizing effect, which appears to scale with total enthalpy normalized by dissociation energy.

New experiments are now under way to extend and consolidate these findings, and to continue with the much more ambitious stability investigation, as well as with a more sophisticated visualization technique.

I.1.1 The experimental setup

The tests were conducted in the hypervelocity shock tunnel T5, which has been adequately described in the proposal for this URI grant. The slender cone used in the experiments is 1 m long and is divided into three sections as shown in Fig. I.1 The tip section (76 mm long) is a solid piece of Waspalloy, a stainless steel that has good toughness at high temperature. Even so, the tip radius was found to increase progressively by melting from shot to shot, from an initial 0.06 mm to approximately 0.15 mm, at which value it stabilizes after typically 20 shots. This increase of nose radius was found to have no detectable effect on the heat transfer distribution.

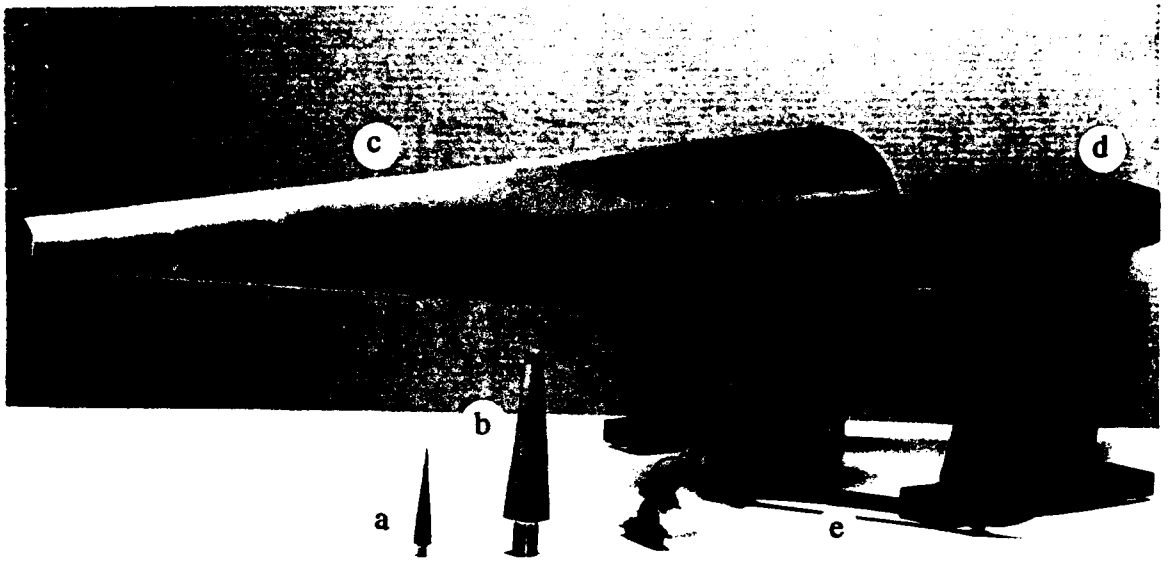

Fig. I.1. Photograph of the model partly disassembled to show the tip (a), the second section (b) and the main body (c). The sting mount is indicated as (d) and the copper pipe protecting the fifteen thermocouple wires as (e).

The second section (127 mm long) is a solid piece of aluminum. The third piece (790 mm long, made of aluminum) is hollow and has a wall thickness of 12 mm. It consists of two longitudinal halves held together by a dove-tail joint, so that they slide into each other without any need for screws, leaving the outside perfectly smooth except for an almost invisible longitudinal seam. The assembled cone is screwed onto a sting-mounted base plate made of steel.

This is mounted rigidly in the test section of T5 after careful alignment of the cone and nozzle axes. The model is positioned in the test section such that it protrudes 330 mm into the nozzle. This allows all the gauges on the cone to be completely inside the uniform test rhombus of the nozzle flow above $M_\infty = 5.6$.

I.1.1.1 Heat transfer gauges

Fifteen thermocouples of type E (chromel-constantan), manufactured by Medtherm Corp., were mounted flush with the surface of the cone to measure the heat transfer distribution. The gauges are placed at approximately logarithmic spacing in axial distance from the tip from 241 mm to 889 mm. Their azimuthal position varies in order to avoid mutual influences, though their flushness is very good. The temperature signal from the gauges is converted to heat transfer by the method of Schultz and Jones (1973). For more detail of the theory of heat flux measurement see section II.2, where the development of improved heat flux gauges is presented.

I.1.1.2 Flow visualization

The main interest in applying flow visualization to this experiment is to study the structure of the transitional and turbulent boundary layer in the high-enthalpy regime. The density and optical path length are too small for regular schlieren, shadowgraphy or interferometry to be sufficiently sensitive to detect the differences in density that occur in the boundary layer because of structure. We therefore resorted to the idea of resonant enhancement of the refractive index of the medium used by Blenstrup *et al.* (1979). This technique relies on the fact that the refractive index of a gas reaches large extrema near a spectral line of the medium. In the visible range, the technique may be implemented by seeding the flow with sodium and using a light source with a wavelength just off the center of one of the D-lines. Even if the light source wavelength is not perfectly tuned, such that it is in the center of the D-line, where the refractive index contribution of the line is zero, the absorption of the light by the resonance is very high. The technique will then still work satisfactorily for qualitative flow visualization with good repeatability.

In our experiment, a preferential enhancement of the sensitivity of the boundary-layer fluid was desirable, so we seeded the flow only within the boundary layer, by depositing a very small drop of a saturated saline solution on the portion of the cone surface of interest. This was then left to dry, so that a thin film of salt was left to be ablated during the test. When dry, the film actually consists of cubic crystals 100 μm high spaced 2 or 3 mm apart.

The light source used was a tunable dye-laser built for this purpose. It is pumped by a Neodymium:YAG laser. Only one picture can be taken during each run. The laser is triggered by an adjustable delay circuit which in turn is triggered by the arrival of the shock at the end of the shock tube.

The resonant enhancement of the refractive index turned out to be particularly successful at high enthalpies (where it was most needed because of the lower density), partially as a result of the relatively higher temperature in the boundary layer, which causes the salt to be ablated more effectively. By control experiments it is found that the disturbance caused by the salt deposition is insufficient to cause the transition location to be moved.

Fig. I.2 shows a schematic diagram of the model, the optical window, and the limits of a typical picture shown in this report. This view is always oriented parallel to the surface of the cone and always shows the flow going from left to right.

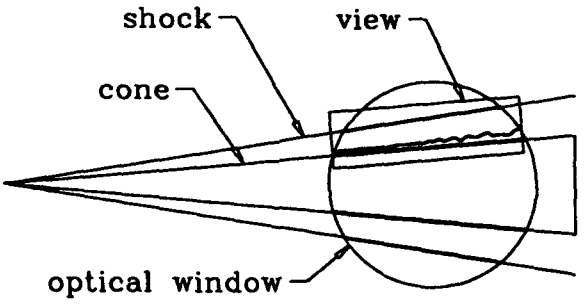

Fig. I.2. Schematic diagram explaining the photographs to be shown below. The flow is always seen going from left to right and the shock is out of the field of view.

I.1.2 Heat transfer in the laminar regime

I.1.2.1 Predictions of similarity theory

The Stanton number is defined as

$$St = \frac{\dot{q}_w}{\rho_e u_e (h_{aw} - h_w)}, \tag{1}$$

where $\dot{q}_w$ is the heat flux to the wall, ρ_e and u_e are density and velocity at the edge of the boundary layer, h_{aw} and h_w are adiabatic and actual specific enthalpy at the wall. To show an example of behavior differences between a frozen flow and a chemical equilibrium flow, we focus on the flow condition corresponding to a specific enthalpy, h_0, of 22 MJ/kg and stagnation pressure, p_0, of 55 MPa. At these conditions, similarity theory gives

$$St_{air} = \frac{0.533}{Pr^{2/3} Re^{1/2}} \quad \text{and} \quad St_{nitrogen} = \frac{0.536}{Pr^{2/3} Re^{1/2}}. \tag{2}$$

If we include the correction factor for real-gas effects (chemical equilibrium),

$$St_{air} = \frac{0.739}{Pr^{2/3} Re^{1/2}} \quad \text{and} \quad St_{nitrogen} = \frac{0.669}{Pr^{2/3} Re^{1/2}}. \tag{3}$$

Re is the Reynolds number evaluated at the edge of the boundary layer and Pr is the Prandtl number. We can also compare these predictions with that of low specific enthalpy (same for air and nitrogen) corresponding to $h_0 = 5.8$ MJ/kg and to $p_0 = 15$ MPa

$$St = \frac{0.487}{Pr^{2/3} Re^{1/2}}. \tag{4}$$

Thus, the frozen cases are almost identical.

I.1.2.2 Experimental results

An example of the normalized experimental results is shown in Fig. I.3 for air. The data shown as squares ($p_0 = 24$ MPa and $h_0 \approx 12$ MJ/kg) indicate a frozen flow behavior as observed by East *et al.* (1980) on a flat plate. The rms error is of order 10%. At high specific enthalpy ($h_0 = 22$ MJ/kg), and higher pressure, the data are more scattered (the rms error is of order 16%) but fall clearly above the prediction of a frozen flow, indicating a higher heat release to the wall because of recombination. The presence of atomic species is due to the combined effect of free-stream dissociation and frictional heating in the boundary layer. The data for air reach a higher level than corresponding data for nitrogen because, at this enthalpy, pure nitrogen does not get dissociated as much as the oxygen in air, so that there is less recombination heat release.

I.1.3 The transitional regime

I.1.3.1 Transition Reynolds

In the example presented in Fig. I.4 and Fig. I.5, the normalized experimental data show that the beginning of the transition Re_{tr} corresponds to a Reynolds number of 2.5-3 million whereas its end corresponds to $Re = 4 - 5$ million. For each run, Re_{tr} is obtained as the intersection of two lines: the first line is a linear fit (of slope –0.5) to the first four data points and the second line is a linear least-squares fit to the data points between this 'laminar line' and the maximum point.

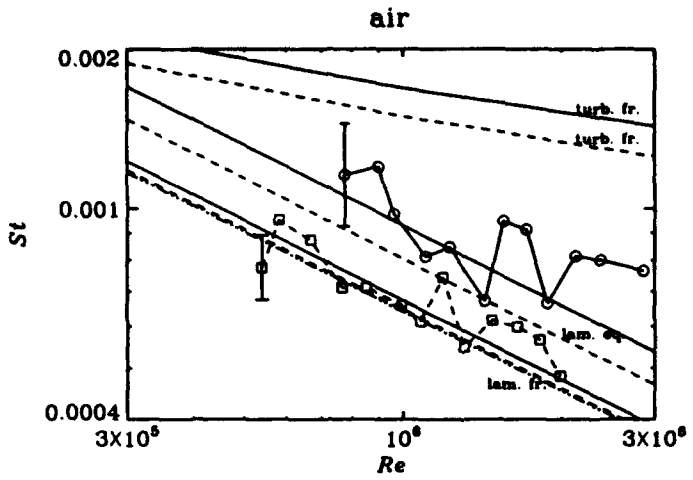

Fig. I.3. Normalized heat transfer results from two different shots in T5. Squares (run 545): h_0 = 11.3 MJ/kg and p_0 = 24 MPa; circles (run 157): h_0 = 18.5 MJ/kg and p_0 = 60 MPa. The theoretical predictions for these air runs are also plotted. ——···——: linear curve fit of experimental data obtained from DiCristina (1970) and from Owen *et al.* (1975). The conditions of their experiments were $h_0 < 1$ MJ/kg and M_∞ = 10 and 7, respectively.

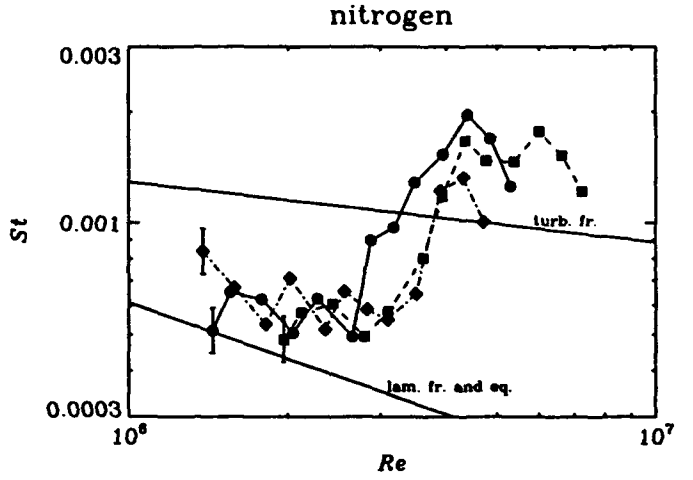

Fig. I.4. Normalized heat transfer data from three different shots in T5. Squares (run 540): h_0 = 7.7 MJ/kg and p_0 = 57 MPa; circles (run 548): h_0 = 9.7 MJ/kg and p_0 = 55 MPa; diamonds (run 534): h_0 = 10.6 MJ/kg and p_0 = 55 MPa. The theoretical predictions for run 548 are also plotted.

In a given facility and at given ambient noise conditions, the transition Reynolds number may be expected to be related to the following dimensionless variables.

$$Re_{tr} = Re_{tr}(M, \gamma, Pr, \frac{T_w}{T_{aw}}, \frac{h_0}{D}, \Omega), \tag{5}$$

where Ω is a dimensionless reaction rate parameter, assuming there is only one D and only one Ω. For example, Demetriades (1977) obtains, for T_w/T_e = 4.2 and 8.4, $Re_{tr} = 3.3 \times 10^6$ and 5.0×10^6,

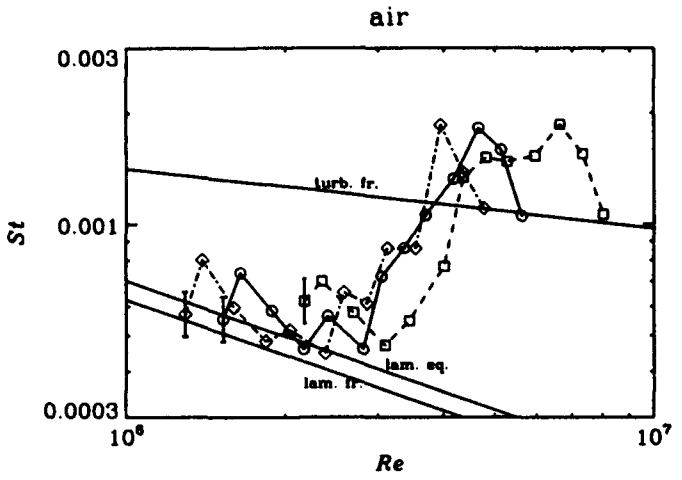

Fig. I.5. Normalized heat transfer measurements of three different shots in T5. Squares (run 541): h_0 = 7.3 MJ/kg and p_0 = 55 MPa; circles (run 549): h_0 = 9.0 MJ/kg and p_0 = 52 MPa; diamonds (run 556, refer to run 537 in Table 2): h_0 = 10.4 MJ/kg and p_0 = 55 MPa. The theoretical predictions for run 549 are also plotted.

respectively. These data and those of DiCristina will be used for comparison purposes[1].

In laminar boundary layers of perfect gases, it is well known that the separate dependence of dimensionless quantities on M, γ, Pr and T_w/T_{aw} disappears if the physical parameters are evaluated at conditions corresponding to the reference temperature T^* introduced by Eckert (1955)[2]. This concept worked very well for the laminar regime on which a dimensionless correction factor, to account for compressibility, was based (Re_{tr} corresponds to the end of the laminar regime). T^* is given by

$$\frac{T^*}{T_e} = 0.5 + 0.039M_e^2 + 0.5\frac{T_w}{T_e}. \tag{6}$$

In an attempt to separate out the real-gas effects, *i.e.*, the influence of h_0/D and of Ω, we renormalized the results for the transition Reynolds number by evaluating it at T^* to give Re^*_{tr}.

$$Re^* = \frac{\rho^* u_e x}{\mu^*}. \tag{7}$$

The results are shown in Fig. I.6 together with the data of DiChristina and Demetriades. As may be seen, our data collapse on two lines: one for air and one for nitrogen.

Clearly, the influence of h_0 on Re^*_{tr} is very significant. Our data extends the enthalpy range of tunnel data from a previous 3 MJ/kg to 15 MJ/kg. Also, the effect of h_0 on the transition Reynolds number is larger if the dissociation energy is smaller. This was further supported by a few experiments performed in carbon dioxide (with a much smaller first dissociation energy and large vibrational energy), which exhibited a much stronger enthalpy dependence, and with helium, for which no enthalpy dependence was observed.

---

[1] Not enough information is provided by Martellucci and Laganelli (1974) to deduce T_w/T_e. Demetriades' (1977) data are all obtained in the same wind tunnel and with the same model.

[2] These conditions should correspond to a reference enthalpy h^* rather than to T^*. For simplicity, we assume that the physical parameters ρ and μ evaluated at T^* are good approximations.

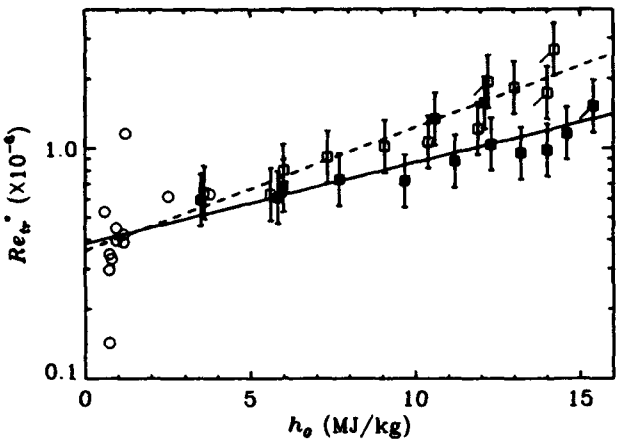

Fig. I.6. Transition Reynolds number evaluated at the reference temperature. Our data are shown as square symbols (open for air and solid for nitrogen). The error bar shown is an approximation of the accuracy in determining Re_{tr}. The data shown as open circles come from DiCristina and Demetriades. The two lines are least-squares-fit approximations of the open or the solid symbols respectively.

I.1.4 Flow visualization

In this section we show examples of flow visualization in the laminar, transitional and turbulent regime. Fig I.7 shows a digitally enhanced small section of the laminar boundary layer, visualized with the resonantly enhanced sodium line technique at a Reynolds number of approximately 1.2 million. The flow is clearly laminar.

Fig. I.7. Flow of nitrogen at $h_0 = 12$ MJ/kg and $p_0 = 24$ MPa (run 544). This resonantly enhanced shadowgraph shows the boundary layer on the top of the 5 deg. half-angle cone at about 570 mm from the cone tip (corresponding to Re = 1.2 million). The horizontal width shown corresponds to approximately 12 mm. In the lower part of the boundary layer the source light is completely absorbed.

In the transitional regime, it is necessary to show a larger extent of the boundary layer. This is done in Fig I.8. As may be seen, the photograph exhibits a waviness at the left, which develops into an almost turbulent boundary layer at the far right of the upper picture. The wavelength (1.5 cm)

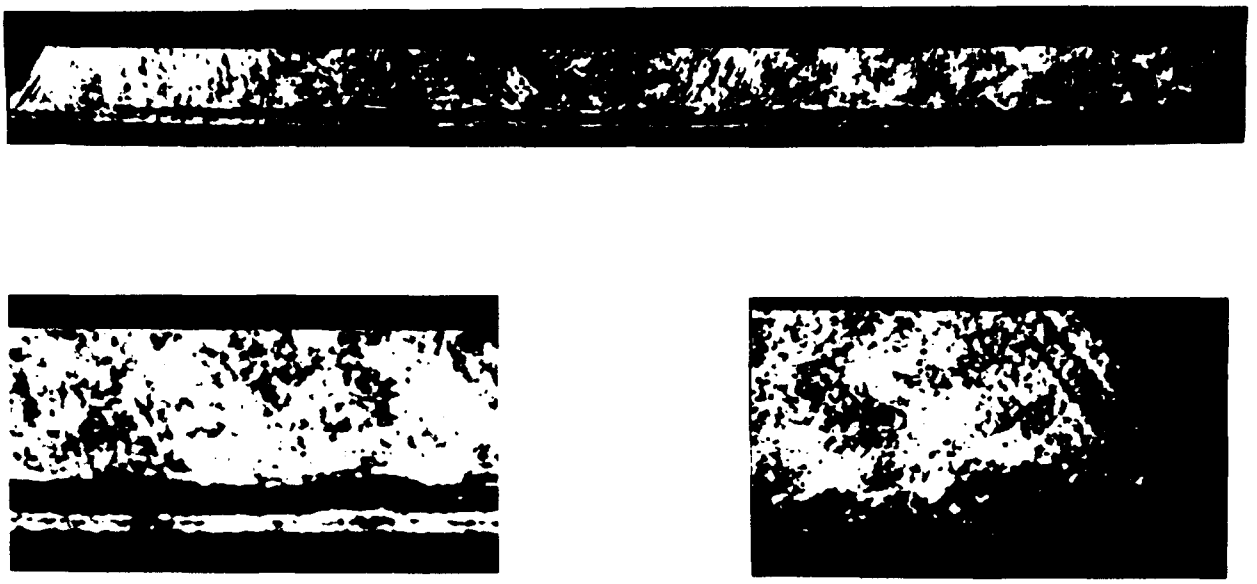

Fig. I.8. Flow of nitrogen at $h_0 = 11$ MJ/kg and $p_0 = 60$ MPa (run 360) This resonantly enhanced interferogram shows the boundary layer on the top of the cone, starting on the left from $x = 510$ mm (corresponding to $Re = 2.75$ million) to $x = 680$ mm ($Re = 3.77$ million). The pictures below magnify portions of the one above three times (3×). A wave in the laminar part of the flow appears distinctly and its wavelength is approximately 1.5 cm.

corresponds approximately to the Tollmien-Schlichting frequency at half the free-stream velocity.

Finally, Fig I.9 shows a turbulent boundary layer that exhibits clear oblique structures that are suggestive of the kind seen in subsonic turbulent boundary layers. The thick viscous sublayer that characterizes cold hypersonic flows is not in evidence at these conditions at all. This may be because the wall-to-reservoir temperature ratio is always very low in these experiments, or because of real-gas effects. However, one also has to be very careful in the interpretation of the pictures, as they are line-of-sight integrating in an axisymmetric flow. Thus, the light beam that passes tangentially to the surface in the vertical centerplane of the cone, also traverses portions of the boundary layer at larger distances from the wall before and after traversing the centerplane.

References

Blenstrup, G., Bershader, D. and Langhoff, P. (1979) "Recent results of resonant refractivity studies for improved flow visualization", *Proceedings of the 12th International Symposium on Shock Tubes and Waves*, Jerusalem, Israel.

Demetriades, A. (1968) "Turbulence measurements in an axisymmetric compressible wake", *Physics of Fluids* **11** (9), 1841-1852.

DiCristina, V. (1970) "Three-dimensional laminar boundary-layer transition on a sharp 8° cone at Mach 10", *AIAA Journal* **8** (5), 852-856.

East, R. A., Stalker, R. J. and Baird, J. P. (1980) "Measurements of heat transfer to a flat plate in a dissociated high-enthalpy laminar air flow", *Journal of Fluid Mechanics* **97**, 673-699.

Fig. I.9. Flow of nitrogen at h_0 = 20 MJ/kg and p_0 = 55 MPa (run 340, refer to 140 in Table 2). This resonantly enhanced interferogram shows the boundary layer on the top of the 5 deg. half-angle cone, starting on the left from x = 420 mm (corresponding to Re = 1.15 million) to x = 590 mm (Re = 1.62 million). The digitally enhanced pictures below magnify portions of the one above three times (3×).

Eckert, E. R. G. (1955) "Engineering relations for friction and heat transfer to surfaces in high velocity flow", *Journal of the Aeronautical Sciences* **22**, 585-587.

Martellucci, A. and Laganelli, A. L. (1974) "Hypersonic viscous flow over a slender cone, Part I: Mean flow mesurements", *AIAA 7th Fluid and Plasma Dynamics Conference, AIAA Paper* 74-533, Palo Alto, California.

Owen, F. K. (1970) "Transition experiments on a flat plate at subsonic and supersonic speeds", *AIAA Journal* 8 (3), 518-523.

Personnel associated with the research

1. Hans G. Hornung, Kelly Johnson Professor of Aeronautics, GALCIT Director.
2. Patrick Germain, Graduate Research Assistant.
3. Eric B. Cummings, Graduate Research Assistant.
4. Philippe Adam, Graduate Research Assistant.
5. Bahram Valiferdowsi, Staff Engineer.

Degrees earned during reporting period

1. Ph. D., Patrick Germain, 1994.

Publications resulting from the research

Germain P, Cummings E and Hornung H (1993) "Transition on a sharp cone at high enthalpy; new measurements in the shock tunnel T5 at GALCIT. AIAA 93-0343, Reno, Nevada.

Germain P, and Hornung H (1993) "The boundary on a sharp cone in high enthalpy flow", Proc. 19th Int Symp on Shock Waves, Marseille, Springer Verlag, to appear.

Germain, P (1993) "The boundary on a sharp cone in high enthalpy flow", Ph. D. thesis, California Institute of Technology.

Hornung H, Wen CY and Germain P (1994) "Hypervelocity flow simulation", Proc Natl Congr. Appl. Mech., Seattle, to appear.

Interactions

Presentations at conferences, see Publications, and at internal seminars and research conferences at Caltech. Presentation at AFWAL workshop. Discussions with R. Kimmel AFWAL, J. R. Maus, E. Edenfield, AEDC, D. Bushnell, G. Anderson, NASA LaRC. Consultant to AEDC, (H. Hornung).

I.2 NONEQUILIBRIUM AND VORTICITY DOWNSTREAM OF BOW SHOCKS

Objectives and Status of the Research

The objectives of this sub-project of the program are to design and execute a series of experiments as well as to perform numerical computations and theoretical analysis, in order to test the nature and limits of binary scaling, and to understand and extend the reaction-rate correlation for the shock-wave stand-off distance, in reacting blunt-body flows. In addition, the experiments are to be extended to investigate the high-vorticity layer downstream of the bow shock that is associated with the large density rise caused by dissociation. The objectives have been extended relative to those in the original proposal because of favorable developments during the reporting period.

An extensive series of experiments on flow over spheres has been completed. This involved nitrogen, air and carbon dioxide flows covering the full range of enthalpy of the hypervelocity shock tunnel T5, ranging from perfect-gas to near-equilibrium flow, and a large range of pressure. Differential interferometry and surface heat transfer constituted the diagnostics used. The experiments were accompanied by detailed numerical computations of the flow fields, which were used to construct interferograms for comparison with the experimental ones. Theoretical analysis of the problem led to a complete understanding of the correlation of the dimensionless stand-off distance with dimensionless reaction-rate parameter, and its extension to reacting gas mixtures. Numerical and experimental results support the correlation very well. A previous theoretical analysis of dissociating flow along a streamline downstream of a curved shock has been extended to include the effects of recombination. The limits of binary scaling were delineated. Initial exploratory experiments on the detection of the high vorticity layer and its stability were performed.

Hypervelocity Flow over Spheres

The nature of the nonequilibrium flow of dissociating gases over spheres was investigated experimentally, numerically and theoretically. A series of experiments with three different gases, nitrogen, air and carbon dioxide, was performed in the shock tunnel T5 at GALCIT. Five spheres of different diameters (1, 2, 3, 4 and 6 in.) equipped with thermocouples for surface heat flux measurements were used. The numerical method by Candler (1988) was used to conduct a parallel study which strongly complemented the experimental and theoretical efforts.

I.2.1 Interferometry and heat flux measurements of blunt body flows

The experimental differential interferograms were compared with the images constructed from computational flow fields. Generally, good agreement of fringe pattern and shock shape was observed. Fig I.10 shows the comparsion of experimental and computational differential interferograms of the flow of nitrogen over a 4 in. diameter sphere at a specific reservoir enthalpy of 16 MJ/kg and a reservoir pressure of 60 MPa. As may be seen, the features of the photo are faithfully reproduced by the computation, both qualitatively and quantitatively in most of the flow field. Small differences near the shock give valuable information about the beginning of the dissociation process.

Experimental heat flux measurements show:

1. Good agreement among the measured stagnation point heat transfer rates, computational results and Fay and Riddell's theoretical predictions. This also provides confirmation of T5 enthalpy

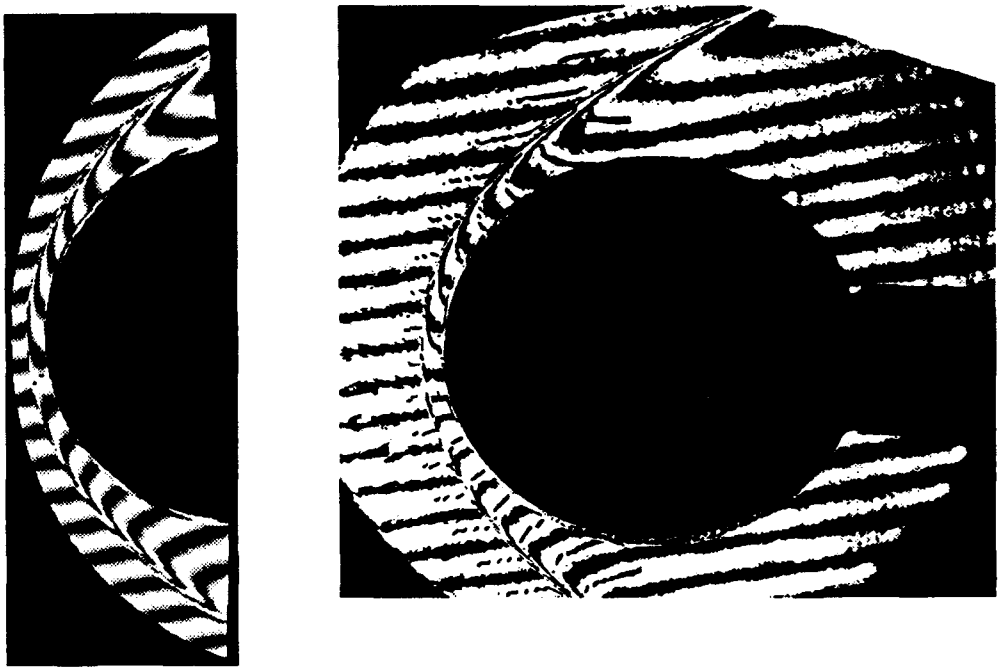

Fig. I.10. Comparison of experimental and computed differential interferograms of nitrogen flow over a sphere. Free-stream conditions: 5.08 km/s, 0.04 kg/m^3, 16.56 MJ/kg. The photograph on the right is a finite-fringe differential interferogram of nitrogen flow over a sphere. The picture on the left is a corresponding computed interferogram at the same conditions as the experiment. Except for a slight difference in the vicinity of the shock, the two pictures are virtually congruent. To show this, a line along the center of the calculated white fringe is superimposed on the photograph.

2. For nitrogen and air, the measured heat flux distributions were also in good agreement with numerical results and Lees' theory.

3. For carbon dioxide, large differences between experimental and theoretical heat flux distributions were observed. Early transition, tripped by surface roughness is a possible cause.

I.2.2 Binary scaling law

An analytical solution was obtained for inviscid hypervelocity dissociating flow over spheres. The solution explains the correlation between the dimensionless stand-off distance and the dimensionless reaction rate parameter previously observed by Hornung (1972) for nitrogen. The physics of the correlation is equivalent to binary scaling. Based on the solution, a new dimensionless reaction rate parameter Ω is defined to generalize Hornung's correlation for more complex gases than nitrogen. The physical meaning of Ω is recognized as the ratio of the energy absorption rate by chemical reactions just after the normal shock to the input rate of free-stream kinetic energy. This suggests that there exists a universal relationship which applies to all gases and free-stream conditions, provided that the Mach number is sufficiently high. The form of the function is also determined by the approximate analysis and is presented together with computational results for air in Fig. I.11 and together with experimental results from T5 for carbon dioxide in Fig. I.12. Experimental and numerical results confirm the new correlation.

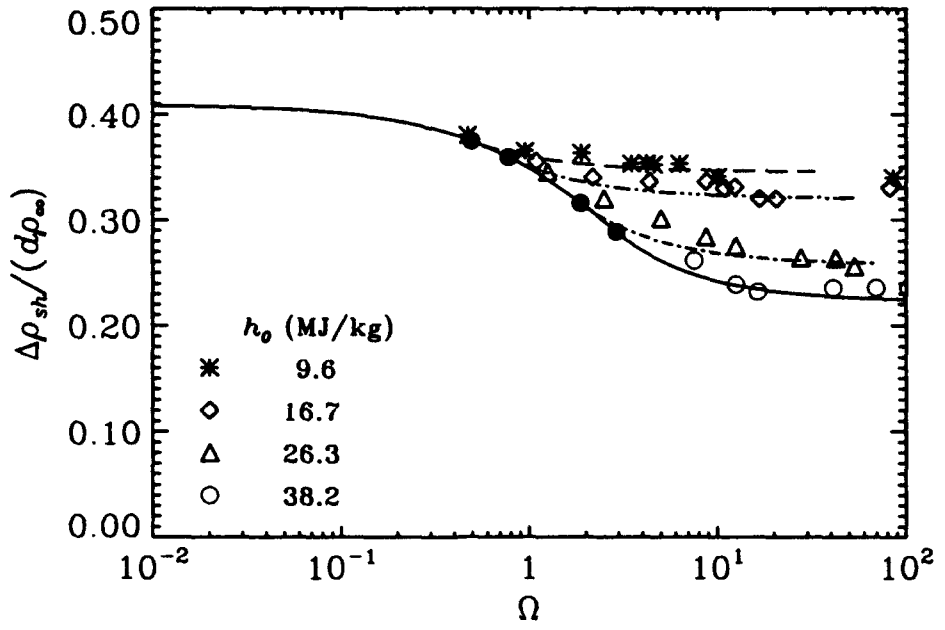

Fig. I.11. Dimensionless stand-off distance plotted against reaction rate parameter for different specific reservoir enthalpies in air. The symbols represent computational results. The filled circle is the point at which the curve branches off from the solid line for each ρ_e/ρ_{sh}.

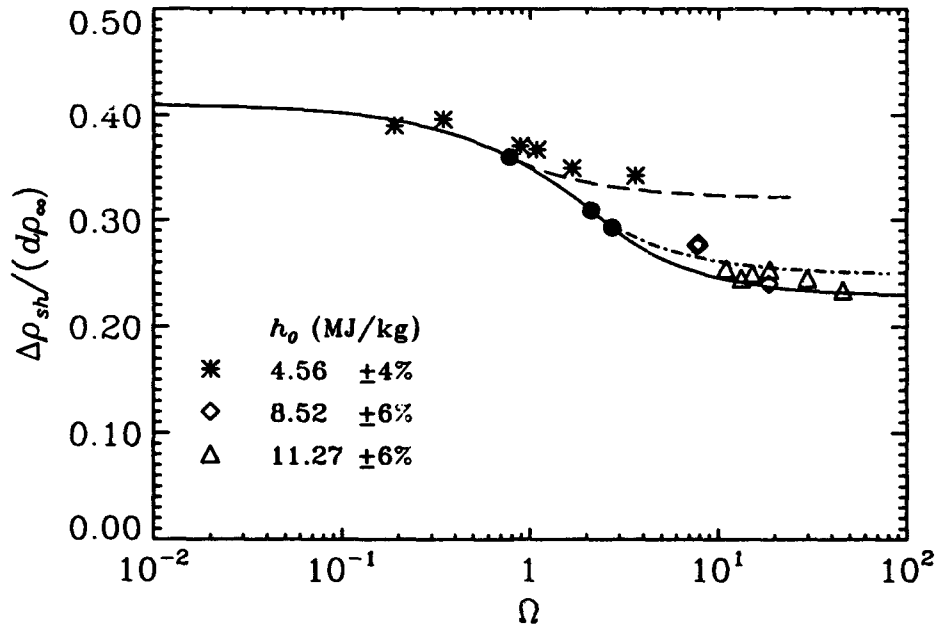

Fig. I.12. Dimensionless stand-off distance plotted against reaction rate parameter for different specific reservoir enthalpies in carbon dioxide. The symbols represent experimental results.

The effect of nonequilibrium recombination downstream of a curved two-dimensional shock was also investigated. An analytical solution for an ideal dissociating gas was obtained, giving

an expression for dissociation fraction as a function of temperature on a streamline. The solution agrees well with the numerical result and provides a rule of thumb to check the validity of binary scaling for the experimental conditions. The effects upon the binary scaling of the large difference in free-stream temperature between flight and free-piston shock tunnel conditions are discovered.

Though theoretical and computational results show that recombination is important in parts of the flow field, binary scaling is a satisfactory model for global quantities such as the stand-off distance.

I.2.3 Vorticity generation by curved shock

Fig. I.13(a) shows a resonantly-enhanced shadowgraph of the carbon dioxide flow. Streamlines are marked by the sodium seeding. At the side of the sphere these show similarities with the instability of a shear layer. Fig. I.13(b) shows these vortical structures on a larger scale. The vortical structures may be the the result of Kelvin-Helmholtz instability of the high-vorticity layer at the edge of the high-entropy layer near the body. If they are, to our knowledge, this resonantly-enhanced shadowgraph is the first visualization of this phenomenon. Further experiments are needed before definite conclusions may be reached. Nevertheless, the resonantly-enhanced shadowgraphic technique provides a promising tool for studying the vorticity-interaction problem in hypervelocity blunt-body flows.

Fig. I.13. Resonantly-enhanced shadowgraph of CO_2 flow over a sphere of 4 in diameter. Free-stream condition: CO_2, 3.55 km/s, 0.081 kg/m^3, 11.27 MJ/kg.

The interaction of the entropy layer and the boundary layer has been a challenging aerodynamic problem for years. The effect of the shock-generated free-stream vorticity on hypersonic boundary layers needs to be understood. Also, experimental and numerical investigations of the real-gas effects in this important feature, both with respect to the amount of vorticity produced by the bow shock, and with respect to the additional amount produced by dissociation downstream of the bow shock are essential to improve the understanding of the fundamental physics in nonequilibrium flow.

Personnel associated with the research

1. Hans G. Hornung, Kelly Johnson Professor of Aeronautics, GALCIT Director.
2. Chih-Yung Wen, Graduate Research Assistant.
3. Patrick Lemieux, Graduate Research Assistant.
4. Bahram Valiferdowsi, Staff Engineer.

Degrees earned during reporting period

1. Ph. D., Chih-Yung Wen 1994.

Publications resulting from the research

[1] Hornung, H.G., Wen, C.Y. and Candler, G.V., "Hypervelocity Flow over Spheres," *Acta Mechanica* [Suppl] 4,163-170, 1994. Also presented at the 3rd International Workshop on Shock Tube Technology, Brisbane and Canberra, Australia, Dec. 1992.

[2] Wen, C.Y. and Hornung, H.G., "Non-Equilibrium Recombination after a Curved Shock Wave," *Proceedings of 1st Pacific International Conference on Aerospace Science and Technology*, Vol. 2, 639-647, Tainan, Taiwan, Dec., 1993.

[3] Wen, C.Y. and Hornung, H.G., "Experiments on Hypervelocity Dissociating Flow over Spheres," *Proceedings of 19th Internation al Symposium on Shock Waves*, Marseille, France, July, 1993, Springer-Verlag, to appear.

[4] Wen, C.Y. and Hornung, H.G., "Hypervelocity Dissociating Flow over Spheres," Submitted to *J. Fluid Mech.*. Also presented at APS Meeting of the Division of Fluid Dynamics, Albuquerque, New Mexico, Nov., 1993.

[5] Olejniczak, J., Candler, G.V., Hornung H.G. and Wen C.Y., "Experimental Evaluation of Vibration-Dissociation Coupling Models", to be presented at AIAA/ASME 6th Joint Thermophysics and Heat Transfer Conference, 1994.

[6] Hornung, H.G., Wen, C.Y. and Germain, P., "Hypervelocity Flow Simulation,", 1994, to be presented at National Congress of Applied Mechanics, Seattle, June, 1994.

Interactions

Presentations at conferences, see Publications, and at GALCIT FLuid Mechanics Seminar and Research Conferences. Discussions with G. Candler, Minnesota, and J. R. Maus, AEDC. Consultant to AEDC, (H.Hornung).

CHAPTER II
SHOCK-VORTICITY INTERACTION

II.1 NONEQUILIBRIUM CHEMISTRY IN SHOCK-VORTEX INTERACTION

Objectives and Status of Research

The objectives of this research are to elucidate the generic mechanisms controlling (1) interaction of a shock wave with a field of vorticity in the presence of nonequilibrium chemistry and (2) vorticity generation mechanisms in shock focusing with reaction chemistry. Progress has been made in computation of steady compressible vortex structures which will then be used as special initial conditions for controlled numerical experiments on shock vorticity interaction. Progress has also been made in developing the computational capability for simulation of vorticity generation through shock focusing. A large scale two dimensional compressible flow solver has been constructed and a high resolution study has been started on two massively parallel machines including the Intel Delta and the IBM SP/1. Finally we have applied Whitham theory to compute an approximation for the vorticity generated by a shock as it interacts with a density gradient. Computations are now in progress to test this approximation.

The next stage of this work will be the use of the steady vortex configurations computed above as initial conditions for our flow simulation and the detailed study of the evolving vorticity distribution. In addition preliminary explorations of the effect of chemistry will be undertaken.

Personnel

(1) D. I. Meiron, Professor of Applied Mathematics.

(2) D. Pullin, Professor of Aeronautics.

(3) Mr. Kayvan Ardalan, graduate student. Thesis will entail study of the properties and stability of steady compressible vortex streets under a variety of boundary conditions

(4) Mr. Mark Meloon, graduate student. Thesis will entail numerical study of vorticity generation through mechanisms of shock focusing, and shock-vortex interactions with reaction chemistry.

II.1.1 Steady Compressible Vortex Arrays

As part of our study of shock-vortex interactions progress has been made towards computing steady compressible vortex solutions. Our plan is to use these solutions as initial conditions and to then examine the shock-vortex interaction resulting from the interaction of an incipient shock with the vortex distribution both in the presence and in the absence of chemistry effects. This approach has the advantage that the vortex distribution is steady and hence one does not have to take into account any time dependence prior to the interaction of the shock with the vortex solution. At present our work has concentrated on two models of steady compressible vortices. The first is an

array of hollow core vortices, an extension of an approach initiated by Moore and Pullin (*JFM*,, 185, 188, 1987). This type of solution is that it allows us to use hodograph techniques which make it possible to apply semi-analytic techniques to effect the solution.

This problem can be formulated by use of the stream function $\psi(x,y)$ such that the velocity field given by $u = \rho^{-1}(\partial\psi/\partial y)$, $v = -\rho^{-1}(\partial\psi/\partial x)$, where ρ is the local density. The hodograph plane method then allows derivation of the Chaplygin equation for ψ

$$q^2\left(1-\frac{q^2(\gamma-1)}{2c_s^2}\right)\frac{\partial^2\psi}{\partial q^2}+q\left(1-\frac{q^2(\gamma-3)}{2c_s^2}\right)\frac{\partial\psi}{\partial q}+\left(1-\frac{q^2(\gamma+1)}{2c_s^2}\right)\frac{\partial^2\psi}{\partial\theta^2}=0,$$

where c_s is the stagnation sound speed. We then determine the image of the row of vortices in the hodograph plane. The main advantage of this approach is that since the velocity on the vortex boundaries must be tangent to the boundaries and since the core is stagnant the hodograph transformation maps the vortex boundary to a straight segment.

We have solved this problem using two complementary approaches. The first is to use the Rayleigh-Janzen method to generate a perturbation solution in powers of the square of the Mach number. This has been completed. We have also set up a numerical approach by solving the Chaplygin equation using finite differences. In order to obtain high resolution we have adopted a capacitance matrix technique which allows us to solve for a solution which satisfies the boundary conditions described above through the modification of a solution which can be obtained using a fast Poisson solver. At present we are comparing the results of this numerical approach along with the Rayleigh-Janzen approach.

The second model is obtained from a continuation of the analytical solutions of Stuart (*J.F.M.*, 29, 417, 1967) for a row of steady *incompressible vortices*, to finite M_∞. This reduces to the solution of coupled nonlinear equations for the density and stream-functions

$$\frac{2\hat{\rho}^2(\hat{\rho}^{\gamma-1}-1)}{\hat{q}_\infty^2(\gamma-1)}+\left(\frac{\partial\hat{\psi}}{\partial x}\right)^2+\left(\frac{\partial\hat{\psi}}{\partial x}\right)^2+\hat{\rho}_\infty\hat{\rho}^2e^{-2\hat{\psi}/\hat{\rho}}=0,$$

$$\frac{\partial}{\partial x}\left(\hat{\rho}^{-1}\frac{\partial\hat{\psi}}{\partial x}\right)+\frac{\partial}{\partial y}\left(\hat{\rho}^{-1}\frac{\partial\hat{\psi}}{\partial y}\right)-\hat{\rho}^{-1}e^{-2\hat{\psi}/\hat{\rho}}=0,$$

where $\hat{\rho}=\rho/\rho_s$, $\hat{q}=q/c_s$, the subscripts "s" and "∞" refer to stagnation conditions and conditions at infinity respectively, and $\hat{\psi}$ is a non-dimensional stream-function. With suitable boundary conditions these equations can be solved by finite difference techniques to yield steady "*compressible Stuart vortex*" solutions of the Euler equations. These can then be used as initial conditions for the unsteady shock-vortex interaction codes. This work is in progress.

II.1.2 Numerical simulation of shock generated vorticity

Several codes for the computation of 2-D unsteady Euler flows have been written, one of which (*PGP2D*: Parallel General Purpose 2D) is ported to the Caltech Intel *Paragon* computer. We describe numerical computations in two space dimensions of Richtmyer-Meshkov instability initiated through the interaction of a propagating shock and a perturbed density gradient. These calculations utilize the EFM numerical technique (Pullin JCP, 34, 231, 1980), a truly multidimensional

algorithm for which the addition of finite-rate chemistry is straightforward. The initial condition is a shock of given Mach number impinging on a density gradient given by

$$\rho = 1 + \beta \left[1 + \tanh \left(\frac{(x - x_l(y))}{\delta} \right) \right].$$

representing a sinusoidally perturbed interface where β is related to the asymptotic density ratio by $\beta = (\rho_2/\rho_1) - 1)/2..$ We take the interface to be given by $x_l(y) = x_0 + A\sin(2\pi ny)$, with $A = 0.1$, $\rho 2/\rho 1 = 2$, $n = 2$, and $\delta = 0.01$. To the left of the layer we place an oncoming shock with shock Mach number of 10. The resolution of the calculations is 400×200 points.

The results of the calculations are displayed in the form of color images in Figures II.1 and II.2. In Figure II.1a-d we display a time sequence of the density. The calculations clearly show the diffraction of the shock as it interacts with the heavier medium down stream. A reflected shock is formed as well which itself focuses as the flow develops. The density gradient displays Richtmyer-Meshkov instability and growth is observed as the layer propagates downstream. Figure II.2a-d displays the corresponding vorticity. One very interesting feature is the production of vorticity of opposite sign in the later stages of the calculation. This is clearly seen for example in Figure II.2d where vorticity of opposite sign to the primary vorticity deposited by the initial interaction of the shock with the density gradient is formed ahead of the density gradient. This is presumably due to shock oscillations of the type seen in our calculations of shock dynamics.

We have also derived a formula to approximate the vorticity generated by the shock using Whitham's shock dynamics. Associated with the formulation of geometrical shock dynamics is the concept of a local flow behind a shock element. We consider the flow at two closely spaced times t and $t + \Delta t$. The idea is to use the formula relating circulation to vorticity as follows:

$$\int_A \omega dA = \int_C \mathbf{u} \cdot d\mathbf{l}$$

where ω is the vorticity contained within the cell, A is the area of the cell, $\mathbf{u}$ is the local velocity along the boundaries of the cell, and $\mathbf{l}$ represents the element of arc along the cell boundary. In using the formula above we assume that the velocities at times $t + \Delta t$ have not changed appreciably from their previous values. This is strictly speaking not true and in order to improve this a better model of the flow behind the shock needs to be developed. The theory of geometrical shock dynamics considers only local fluid effects in order to determine the motion of the shock. An improved theory has been developed recently by J. P. Best and it would be of interest to determine if this could be used to provide improved values of the vorticity, but this has not been implemented here. The result of this calculation is

$$\omega = \frac{1}{a_0 M} \frac{d}{de} \left(\frac{2a_0^2(M^2 - 1)}{\gamma + 1} \right)$$

where a_0 is the local sound speed ahead of the shock and M is the local shock Mach number. Note that this result implies there are two ways in which vorticity is generated. The first is through the variation of the sound speed along the shock. This would occur for example if the shock encounters a density gradient. The second is through variations of the Mach number along the shock. This implies that the shock is curved. Both these mechanisms are known to generate vorticity in compressible flow through the interaction of the misaligned density and pressure gradients. Note also that no vorticity is generated in the absence of these conditions. Further computations are now in progress to compare the actual vorticity levels predicted by shock dynamics with those of the full calculation.

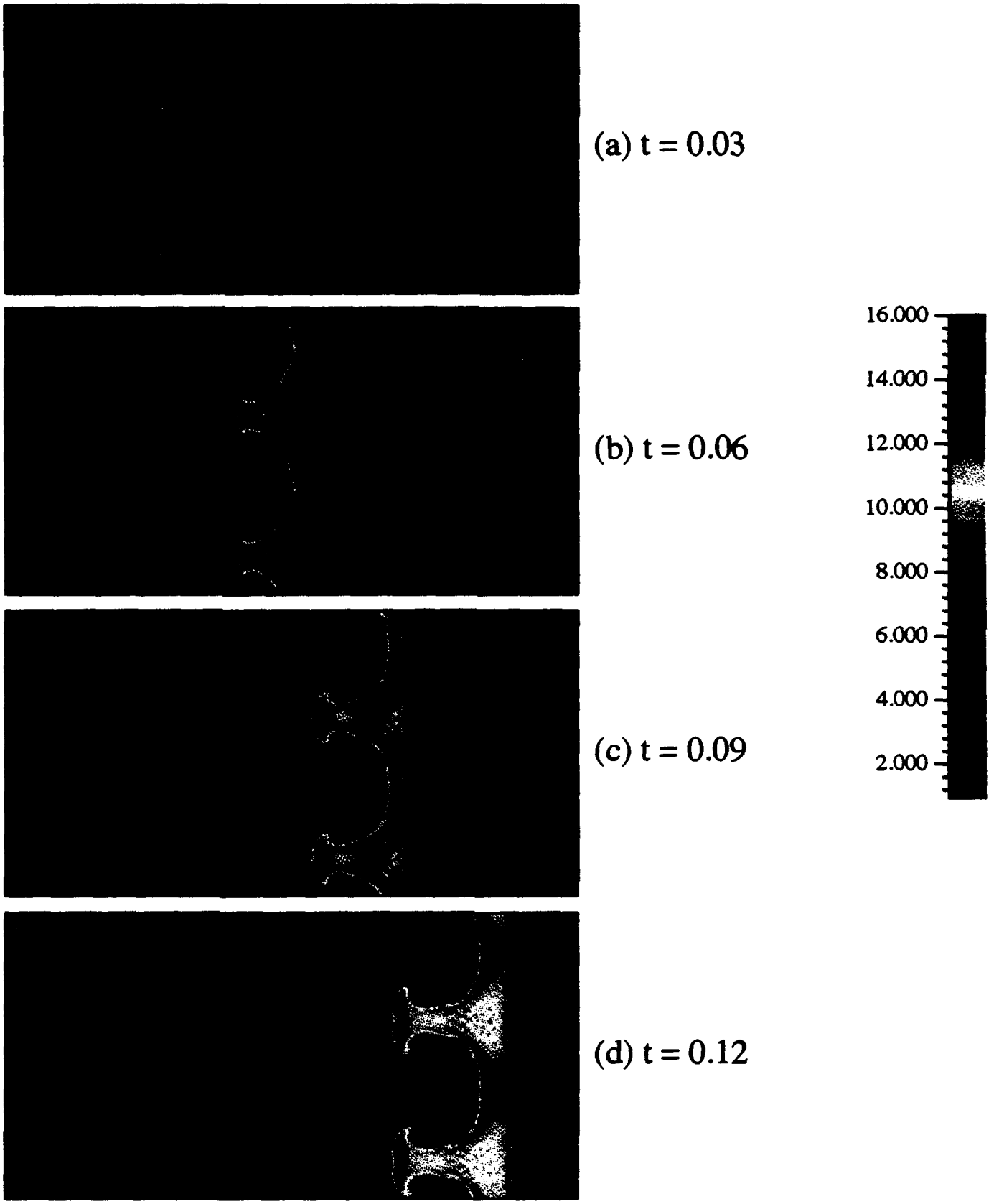

Figure II.1: Shock-density gradient interaction, M=10.
Time sequence of color coded density field

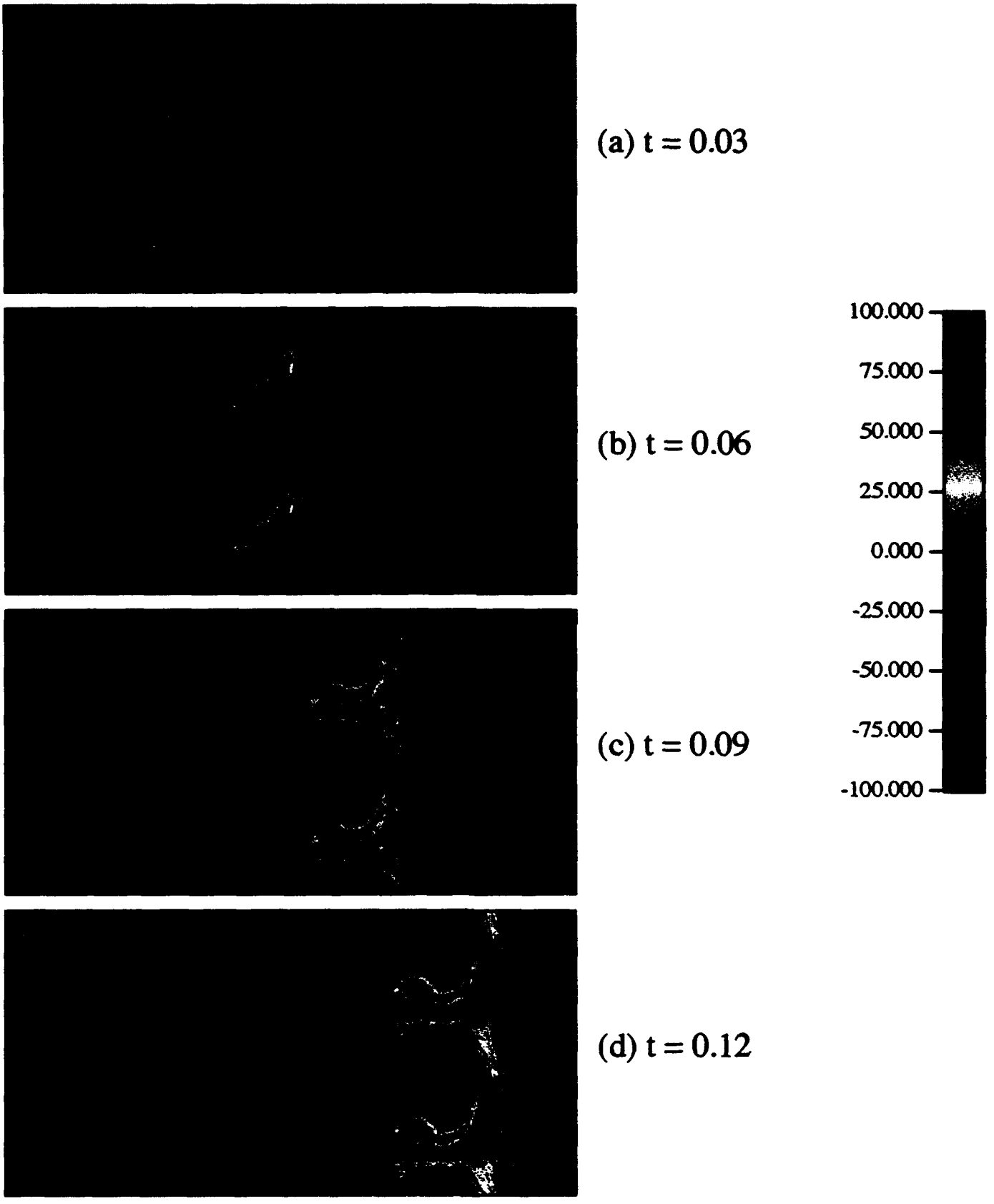

Figure II.2: Shock-density gradient interaction, M=10.
Time sequence of color coded vorticity field

II.2 SHOCK WAVE INTERACTIONS IN HYPERVELOCITY FLOW

Objectives and Status of Research

The objective of this experimental study is to determine the effects of chemical relaxation on the shock-on-shock problem, and, in particular, to quantitatively demonstrate the magnitude of nonequilibrium effects on shock impingement heating. Preliminary experiments in T5 were described in the proposal for this grant and in Ref. 1. Presently, cylindrical and spherical models are being constructed for a new series of tests. Modifications are required to the impinging-shock generators (items B.1 and 2, Statement of Work; Design and construct shock generators), and the three T5 test conditions established for this project are being refined.

The primary effort during this reporting period was to make major improvements in methods for heat transfer measurement and optical interferometry in T5. In addressing item A.3, Statement of Work (Improve existing Wollaston prism differential interferometer), a more sweeping solution was sought; a completely new holographic system for optical diagnostics in T5 has been designed and built. This instrument will be reported at another time. In this report we document the development of a new heat transfer gauge which gives performance superior to any existing device.

II.2.1 A surface junction thermocouple sensor for transient heat flux measurements

The measurement of heat transfer rates to aerodynamic surfaces is important in the design of thermal protection for hypervelocity aerospace vehicles. These flows may be created in wind tunnels for only a fraction of a second, due to the high specific energies involved and the limited strength of materials at elevated temperatures. Thus the problem is transient in nature and a common measurement technique is to sense the time history of the surface temperature of the model. The unsteady conduction of heat within a solid body is described by linear partial differential equations and so the heat transfer rates at the surface of a body may be inferred from the surface temperature measurements. The operating principles, and typical sensor designs are described by Schultz and Jones (1973).

We have conducted experiments in the T5 free piston driver shock tunnel at GALCIT. This facility is capable of simulating the high density hypervelocity flows about space vehicles at speeds of order 5000 m/s. Under these extreme conditions the flow in typical facilities is contaminated with the products of mechanical, physical and chemical breakdown of a variety of metallic and nonmetallic materials. Some erosion of the surface of the gauge is probable under these conditions and this impacts the design of the transducer.

A commonly used technique for gauge fabrication is to deposit a thin metal film (typically Platinum) on a glass or ceramic substrate. The surface temperature is then sensed through the temperature dependence of the resistivity of the metal film. This technique yields a relatively sensitive device however the thin film is prone to damage in hostile environments. Any erosion of the metal film alters the sensitivity of the gauge and so these devices are unsuitable for some wind tunnels. Observe also that since the sensitivity of the gauge depends on the geometry of the device, calibration of each individual sensor is required.

An alternative physical mechanism for temperature measurement is the thermoelectric EMF

produced at a junction of dissimilar metals. If a metallic substrate is used, the gauge is capable of tolerating a larger transient heat flux due to the higher thermal diffusivity and the larger allowable temperature. The figure of merit is $T_{max}\sqrt{\rho ck}$ [see Eqn. (4)]. A particularly robust design results when the thermocouple material itself is used as the substrate. The sensitivity of the gauge is then unaffected by surface erosion or gauge geometry and depends only on physical properties of the materials. Thus calibration of individual gauges is not required.

The design problem in producing such a gauge is to insulate the two conductors that form the thermocouple so that only a thin surface junction is formed. Common practice is to construct the gauge from coaxial cylindrical thermocouple elements that are insulated by a layer of epoxy or ceramic adhesive. The surface junction is formed by electrolytic deposition of a metal film or by abrasion of the exposed surface. In either case very fine tolerances are required to produce a small gap between the thermocouple elements and the effective depth of the junction scales with the width of the gap between the conductors. Note that as the test time is reduced, a thinner junction is required for the same materials.

II.2.2 Analysis of heat conduction in gauge substrate

In order to illustrate the principles of gauge operation and to assess the effect of the finite thickness of the surface junction, consider the unsteady conduction of heat in a one-dimensional semi-infinite solid. For small temperature gradients this process is described by the usual linear partial differential equation,

$$\frac{\partial^2 T}{\partial x^2} = \frac{1}{\alpha}\frac{\partial T}{\partial t}; \qquad \alpha = \frac{k}{\rho c}, \tag{1}$$

where T is the temperature, x is the spatial coordinate normal to the surface, t is time and α is the thermal diffusivity, k is the thermal conductivity, ρ is the density and c is the specific heat of the material. For the following uniform initial condition, T_i, and instantaneously applied, constant surface heat flux, $\dot{q}_0$;

$$T(x,0) = T_i,$$

$$\left(\frac{\partial T}{\partial x}\right)_{x=0} = \frac{-\dot{q}_0}{k}; \qquad t > 0,$$

the solution is,

$$\Delta T = T - T_i = \frac{2\dot{q}_0}{k}\sqrt{\frac{\alpha t}{\pi}}\exp\frac{-x^2}{4\alpha t} - \frac{\dot{q}_0 x}{k}\left(1 - \operatorname{erf}\frac{x}{2\sqrt{\alpha t}}\right). \tag{2}$$

Expanding this solution asymptotically in powers of t as $t \to \infty$ at constant x we obtain,

$$\Delta T = 2\frac{\dot{q}_0}{k}\sqrt{\frac{\alpha}{\pi}}t^{\frac{1}{2}} - \frac{\dot{q}_0}{k}x + \frac{1}{2}\frac{\dot{q}_0}{k}\frac{1}{\sqrt{\alpha\pi}}x^2 t^{-\frac{1}{2}} + O\left(t^{-\frac{3}{2}}\right) \tag{3}$$

Further, the first term is asymptotically dominant for $\frac{x}{(\alpha t)^{\frac{1}{2}}} << 1$.

$$\Delta T \asymp 2\frac{\dot{q}_0}{k}\sqrt{\frac{\alpha}{\pi}}t^{\frac{1}{2}}, \tag{4}$$

and this expresses the usual result that the surface temperature rises parabolically with time for a constant heat flux. The criterion $\frac{x}{(\alpha t)^{\frac{1}{2}}} << 1$ provides a limit on the thickness of the surface sensing element for practical designs. The next order term, $\frac{\dot{q}_0}{k}x$, gives the error in the surface temperature measurement associated with this finite thickness and the estimate is also asymptotically valid provided $\frac{x}{(\alpha t)^{\frac{1}{2}}} << 1$. Extracting the exponential prefactor and expanding asymptotically as $t \to 0$ at constant x, the leading order behavior is;

$$\Delta T \asymp \frac{4\dot{q}_0}{kx^2}\left(\frac{\alpha t}{\pi}\right)^{\frac{3}{2}} \exp\frac{-x^2}{4\alpha t}; \qquad \frac{x}{(\alpha t)^{\frac{1}{2}}} >> 1. \tag{5}$$

Hence at small times the temperature rises exponentially fast. The significance of the various terms of the expansion is illustrated in Fig. II.3 At long times the solution asymptotes to the true surface temperature, given by the first term in the expansion (3), with a constant error given by the second term of (3). This error becomes small with respect to the true surface temperature provided $\frac{x}{(\alpha t)^{\frac{1}{2}}} << 1$.

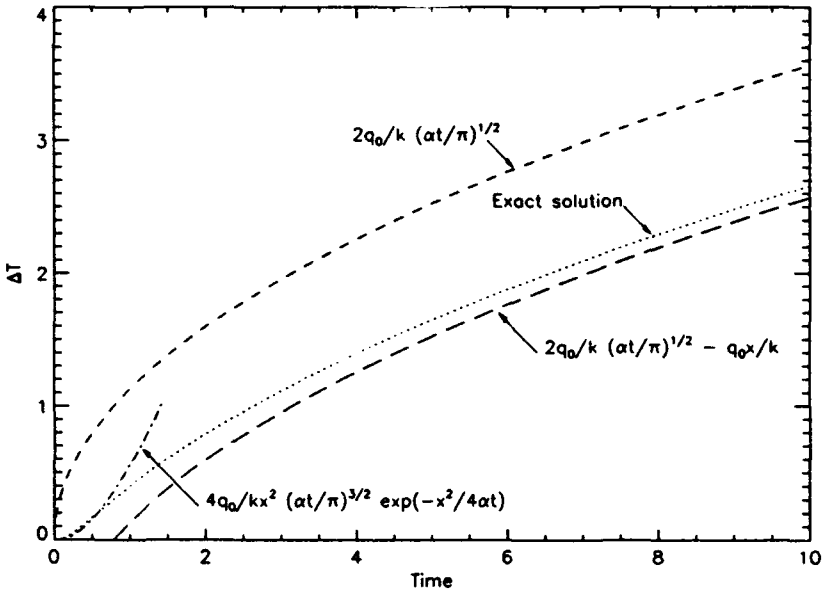

Fig. II.3. — Asymptotic behavior of a surface temperature sensor. For illustrative purposes $\alpha = 1$, $k = 1$, $\dot{q}_0 = 1$, $x = 1$.

II.2.3 Description of new gauge design

A new gauge design has been developed and tested with the aim of simplifying the construction of surface junction thermocouple sensors. The essential feature of this design is the use of a slightly tapered center conductor. The resulting interference between the tapered center pin and the sharp edged outer conductor forms a thin surface junction and provides reliable insulation (see Fig. II.4). The protruding pin is severed and the surface is polished once the gauge has been assembled.

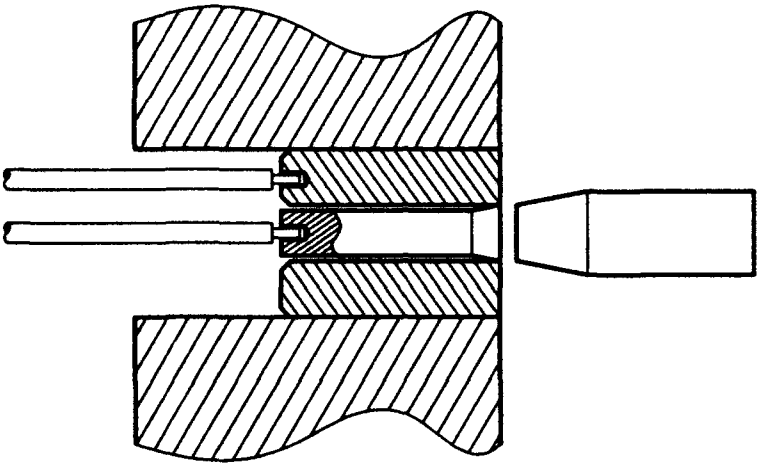

Fig. II.4. Layout of new surface junction thermocouple sensor.

This design results in a robust transducer whose sensitivity is determined solely by the physical properties of the thermocouple materials. There is a further weak dependence on the taper angle however this is constant for all gauges and is determinable by either calibration or analysis.

The effective thickness of the junction may be estimated from the surface roughness of the thermocouple components and the taper angle of the center conductor (see Fig. II.5). The thickness of the junction, averaged over the two surfaces may be estimated to be,

$$\text{thickness} = \text{taper} \times \text{roughness}.$$

It is possible to achieve a 0.3 μm finish with conventional machining operations and with a 5:1 taper the average junction depth is 1.5 μm. For the gauges described here type E (Chromel - Constantan) thermocouples were used and the average thermal diffusivity for these materials is $5 \times 10^{-6}\ m^2/s$. A response time of 0.5 μs then follows from the condition $\frac{x}{(\alpha t)^{\frac{1}{2}}} << 1$. The test time for typical hypervelocity wind tunnels lies in the range 1–100 ms and so this is acceptable. The length of the gauge must be sufficient such that the temperature rise at the rear surface is negligible. This is determined from the condition $\frac{x}{(\alpha t)^{\frac{1}{2}}} >> 1$; where here the scales are understood to be the test time and the length of the gauge.

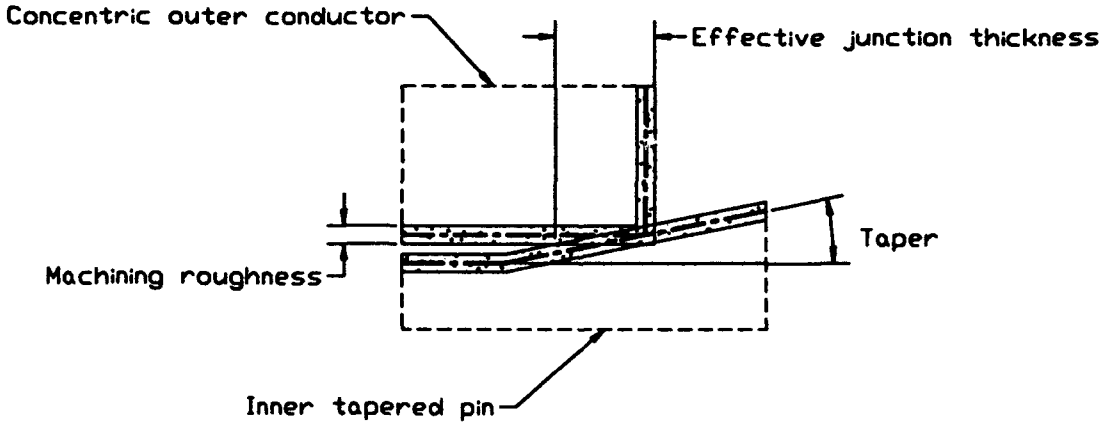

Fig. II.5. Effective thickness of thermocouple junction.

A second dissimilar metal junction is formed between the outer conductor and the model. This junction extends along the full length of the gauge since these surfaces are not insulated and so the thermoelectric EMF is small. This common mode EMF and noise pickup are reduced by the use of a relatively crude differential amplifier (see Fig. II.6). The cold junction is formed at ambient temperature at the circuit board. This arrangement is adequate given the constancy of the cold junction temperature during the short run time and the large hot junction temperature rise experienced in hypervelocity wind tunnels (approx. 200K).

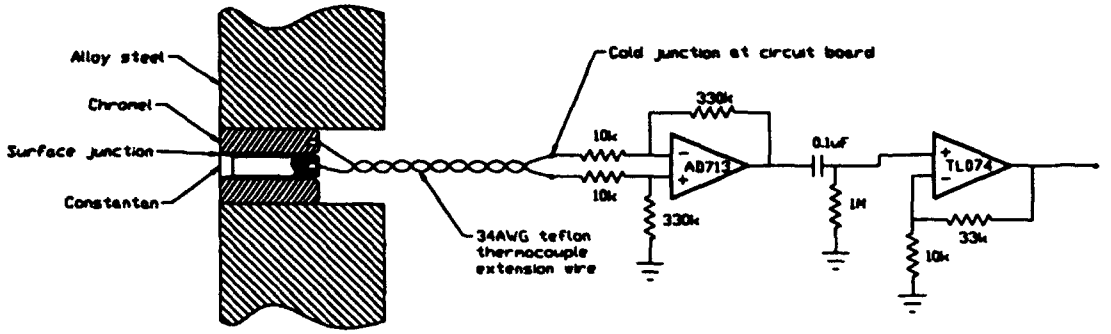

Fig. II.6. Schematic of amplifier circuit.

The center pin is located in the concentric outer conductor and secured with epoxy or ceramic adhesive. Sufficient force is applied to ensure adequate registration of the mating parts however care must be taken not to deform the edge of the outer conductor. Thermocouple extension wires are resistance welded to the rear of the assembly by discharging a capacitor through the wire. The thermocouple is then installed flush with the outer surface of the model and the protruding center pin is removed. The excess material is removed by filing and the surface is honed to produce the surface junction. It is helpful to apply a small amount of Prussian blue to the surface of the thermocouple and once this is just removed by filing, the formation of a thin junction is assured. It is advisable to manufacture the model from a material somewhat harder than the thermocouple material so that the model contours are not altered during this process. It is possible for test section models to experience surface temperature rises of 1000K during the short test time. Degradation of the adhesive bond between the conductors will also occur however the penetration depth during the test time is small relative to the overall length of the gauge and the bond at the rear maintains the integrity of the device.

II.2.4 Deducing the surface heat transfer rate

If the unsteady conduction of heat in the thermocouple sensor is modeled by the analysis presented in §II.2.2 then given the time history of the surface temperature and the physical properties of the gauge materials it is possible to solve an inverse problem for the time history of the surface heat flux. The procedure is described by Schultz and Jones (1973) whereby the calculation is performed using a problem specific quadrature scheme or by an electronic analogue.

Observe however that the governing equations are linear and hence the dynamic behavior of such a system may be generally be described by a convolution integral,

$$\Delta T(x,t) = \int_0^t g(x,t-\tau)\dot{q}(\tau)d\tau. \tag{6}$$

The unit impulse response function, $g(x,t)$, is given by the derivative of Eqn. (2),

$$g(x,t) = \frac{\partial \Delta T(x,t)}{\partial t} = \sqrt{\frac{\alpha}{\pi k^2 t}} \exp \frac{-x^2}{4\alpha t}; \qquad t > 0. \tag{7}$$

Note that the integral (6) is improper in the limit $x \to 0$ and a finite value of x is taken to regularise the problem (as estimated in §II.2.2). Recasting the problem in this general form allows the use of spectral deconvolution methods that provide a mean square optimal estimate of the time history of the surface heat flux. This procedure provides optimal rejection of the errors associated with the differentiation of noisy experimental data. Theoretical background is given in Papoulis (1984) and the numerical implementation with discrete Fourier transform algorithms is described by Press *et al* (1988). A concise description of these methods applied to an analogous problem is given by Sanderson and Simmons (1991).

If the noisy experimental data in discrete time is,

$$z_i = \Delta T_i + n_i, \tag{7}$$

then the deconvolution problem comprises determining the acausal filter, ϕ_i, that gives a mean square optimal estimate, $\dot{q}_i^*$, of the time history of the surface heat flux. Thus,

$$\sum_{k=0}^{N-1} \phi_{i-k} z_k = \sum_{k=0}^{i} g_{i-k} \dot{q}_k^*; \qquad i = 0, 1...N-1. \tag{8}$$

By the convolution property of the discrete Fourier transform, and since $g_i = 0$ for $i < 0$,

$$\Phi_j Z_j = G_j \dot{Q}_j^* \qquad j = 0, 1...N-1. \tag{9}$$

It may be shown that the optimal filter is approximated by,

$$\Phi_j = \frac{S_{ZZ_j} - \nu_j}{S_{ZZ_j}}, \tag{10}$$

where S_{ZZ_j} is the discrete power spectral density of the surface temperature measurement and ν_j is the power spectral density of the signal noise. By inverse discrete Fourier transform, the optimal estimate of the surface heat flux is then,

$$\dot{q}_i^* = F^{-1}\left[\frac{\Phi_j Z_j}{G_j}\right]; \qquad i, j = 0, 1...N-1. \tag{11}$$

Note that all time series must be padded to twice their length with trailing zeroes to enforce causality of the right hand side of Eqn. (8) when discrete Fourier transforms are used in this manner.

II.2.5 Experimental results

In order to demonstrate the performance of the new heat transfer gauge we have measured the stagnation point heat transfer rate to a $50mm$ diameter sphere in hypervelocity flow. Fig. II.7 shows the time history of the nozzle reservoir pressure, test section pitot pressure, stagnation point surface temperature and the stagnation point heat transfer rate deduced from it.

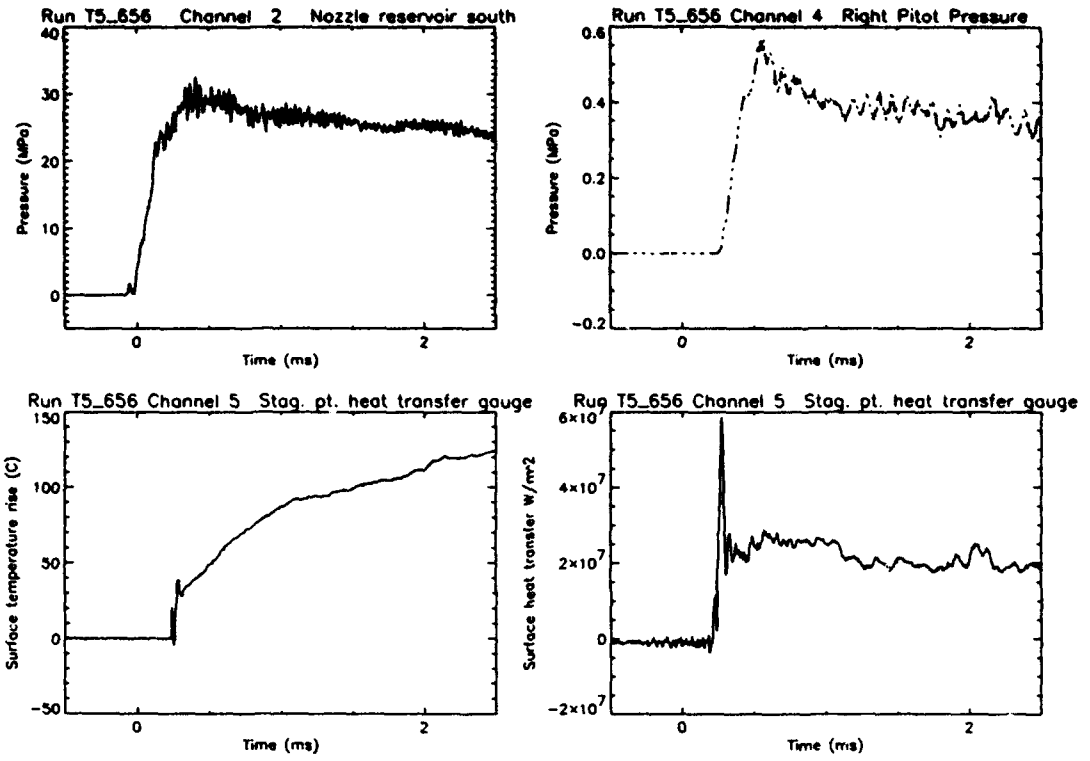

Fig. II.7. Stagnation point heat transfer measurement for sphere in hypervelocity flow. The free stream conditions are $\rho = 0.020\text{kg/m}^3$, $u = 4590\text{m/s}$, $T = 1700\text{K}$, $p = 10.4\text{kPa}$, $M = 5.65$, $h_0 = 13.2\text{MJ/kg}$ and these are computed from measurements of the shock tube filling pressure, primary shock speed before reflection and the nozzle reservoir pressure.

II.2.5.1 Accuracy of measurements — general considerations

The repeatability of the measurement has been established by repeating the condition corresponding to Fig. II.7 with a different gauge of the same design and these results are illustrated in Fig. II.8. The flow environment is extremely hostile and since the thermocouple junction is electrically exposed to the flow it is necessary to demonstrate that erroneous EMFs are not generated by physical mechanisms other than the thermoelectric effect. A dummy gauge of identical design was manufactured with both conductors made of Constantan and so no thermoelectric EMF should be generated. Fig. II.9 shows the results obtained with this dummy gauge at a high enthalpy condition. Apart from an initial transient that decays rapidly, no erroneous EMFs are discernible on this scale. The deconvolved heat transfer rate is three orders of magnitude less than the actual heat transfer rate.

The conversion from thermoelectric EMF to temperature is given by the standards for type-E thermocouples within prescribed error limits. Further errors associated with the uncertainty in the physical properties of the thermocouple elements, the difference in α and k for the two dissimilar metal conductors and the reduced heat conduction away from the surface due to tapering of the center conductor may be eliminated by calibration. The tapering of the Constantan pin effectively reduces its thermal diffusivity and this error tends to negate the unavoidably lower thermal diffusivity of Chromel. These systematic errors may be eliminated by calibration to any desired level of accuracy. The remaining systematic error due to the finite thickness of the surface

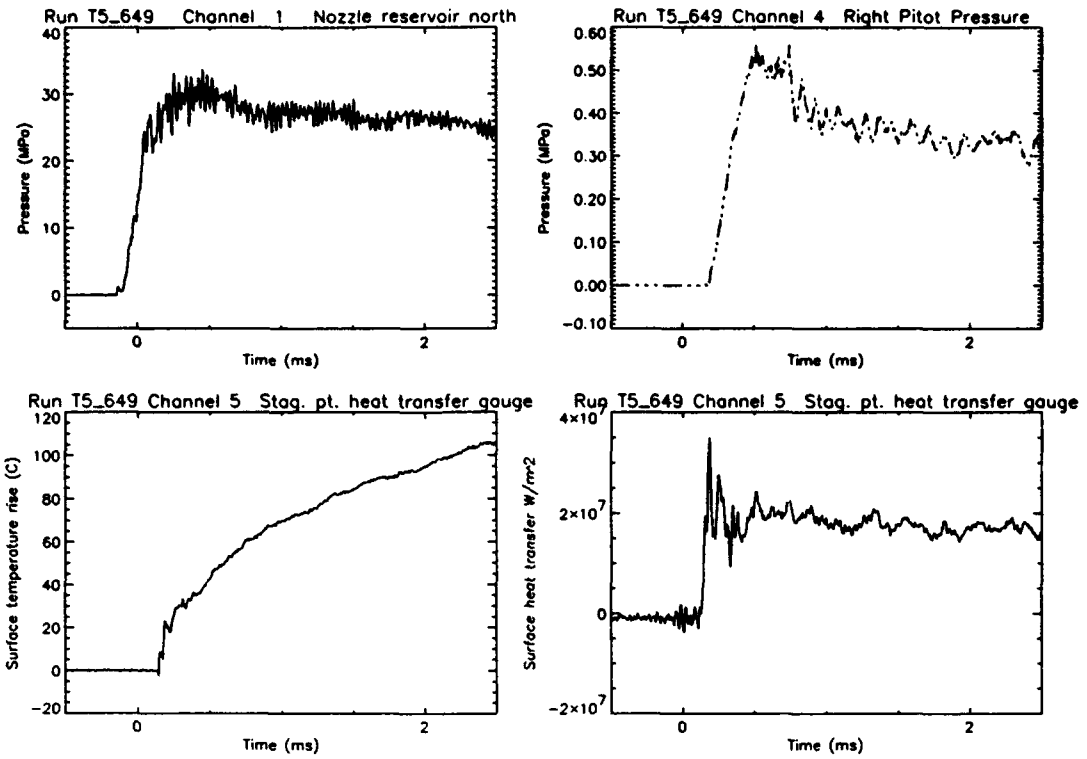

Fig. II.8. Stagnation point heat transfer measurement for sphere in hypervelocity flow. The free stream conditions are nominally identical with those for Fig. II.8

junction may be estimated from the preceding analysis.

II.2.5.2 Accuracy of measurements — high heat transfer rates

The surface temperature rise of models in T5 may easily exceed several hundred Kelvin. Under these conditions the physical properties of the thermocouple materials change significantly with temperature. Particularly strong variations of the specific heat are possible in the vicinity of solid state phase transitions. Metastable phases that may arise under conditions of rapid heating and cooling pose further difficulties. Existing analyses for deducing the model heat transfer rate from the surface temperature time history are based on linear hypotheses. Some literature exists for estimating the errors associated with the quasi-linear temperature dependence of the material properties [Schultz and Jones (1973), Hartunian and Varwig (1962)]. The issue of genuine non-linearity associated with phase transitions remains open. The lack of reliable data and the difficulty of obtaining it through calibration pose further problems. Consequently, analysis of these effects will initially be limited to an estimation of errors.

II.2.6 Conclusions

A new surface junction heat transfer gauge has been developed and its use demonstrated by the measurement of the stagnation point heat flux for a sphere in a reacting supersonic flow. The repeatability and validity of the measurements in a hostile flow environment has been demonstrated. Analysis has illustrated the principle of operation and spectral methods were used to infer the surface heat flux from surface temperature measurements. Potential error sources were identified.

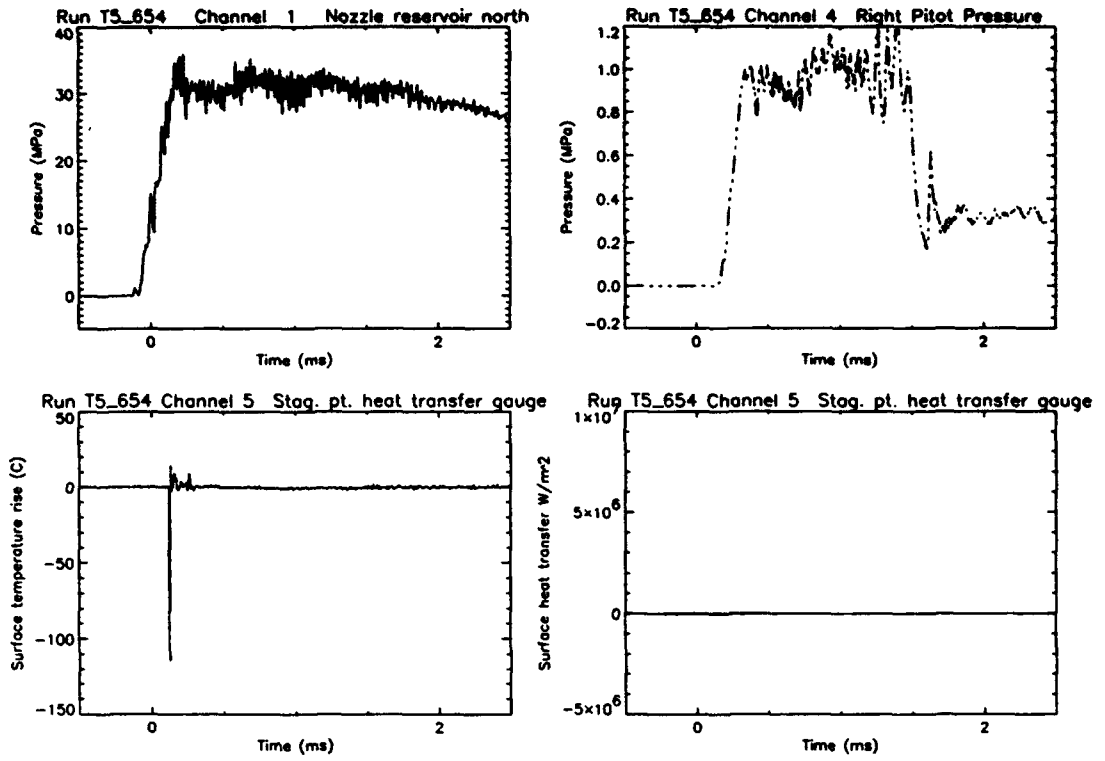

Fig. II.9. Stagnation point heat transfer measurement for sphere in hypervelocity flow, using dummy Constantan – Constantan thermocouple. The free stream conditions are $\rho = 0.018\text{kg/m}^3$, $u = 5300\text{m/s}$, $T = 2320\text{K}$, $p = 13.7\text{kPa}$, $M = 5.52$, $h_0 = 19.6\text{MJ/kg}$ and these are computed from measurements of the shock tube filling pressure, primary shock speed before reflection and the nozzle reservoir pressure. (The large drop in the pitot pressure at $t = 1.5\text{ms}$ is intentionally caused by the passage of an oblique shock wave.)

References

1. Sanderson, S.R. and Sturtevant, B. (1994), Shock wave interactions in hypervelocity flow, 19th Int'l. Symp. on Shock Waves, Marseille, July, 1993

2. Fay J.A. and Riddell F.R. (1958), Theory of stagnation point heat transfer in dissociated Air, *Journal of the Aeronautical Sciences*, **25**(2), pp. 73–85.

3. Hartunian R.A. and Varwig R.L. (1962), On thin-film heat-transfer measurements in shock tubes and shock tunnels, *Physics of Fluids*, **3**(2), pp. 169–174.

4. Papoulis A. (1984), *Probability, Random Variables and Stochastic Processes*, Mc-Graw Hill.

5. Press W.H., Flannery B.P., Teukolsky S.A. and Vetterling W.T. (1988), *Numerical Recipies in C*, Cambridge University Press.

6. Sanderson S.R. and Simmons J.M. (1991), Drag balance for hypervelocity impulse facilities, *AIAA J*, **29**(12), 2185.

7. Schultz D.L. and Jones T.V. (1973), *Heat-transfer Measurements in Short-duration Hypersonic Facilities*, AGARDograph No. 165.

Publications Resulting from Research

Sanderson, S.R. and Sturtevant, B. 1994 Shock wave interactions in hypervelocity flow, 19th Int'l. Symp. on Shock Waves, Marseille, July, 1993

Personnel Associated with Research

1. B. Sturtevant, Professor of Aeronautics.
2. Simon R. Sanderson, Graduate Student.
3. Bahram Valiferdowsi, Staff Engineer.

Interactions

1. Attended 19th International Symposium on Shock Waves, Marseille, July, 1993, at which 400 shock-wave specialists met.
2. Attended 3rd International Workshop on Shock Tube Technology, Brisbane, December 1992.

CHAPTER III
SUPERSONIC SHEAR-LAYER FLOWS

III.1 Bi-supersonic shear-layer flows

During the past year, the GALCIT Supersonic Shear Layer (S^3L) facility was upgraded to permit operation in a bi-supersonic flow regime, *i.e.*, both freestreams supersonic. Investigation of this fully-hyperbolic flow regime will allow us to address a host of important issues, such as the influence of upstream and downstream boundary conditions, the interaction of shock waves with the turbulent mixing zone, and the effect of new compressibility phenomena in both chemically-reacting and non-reacting gas-phase flows.

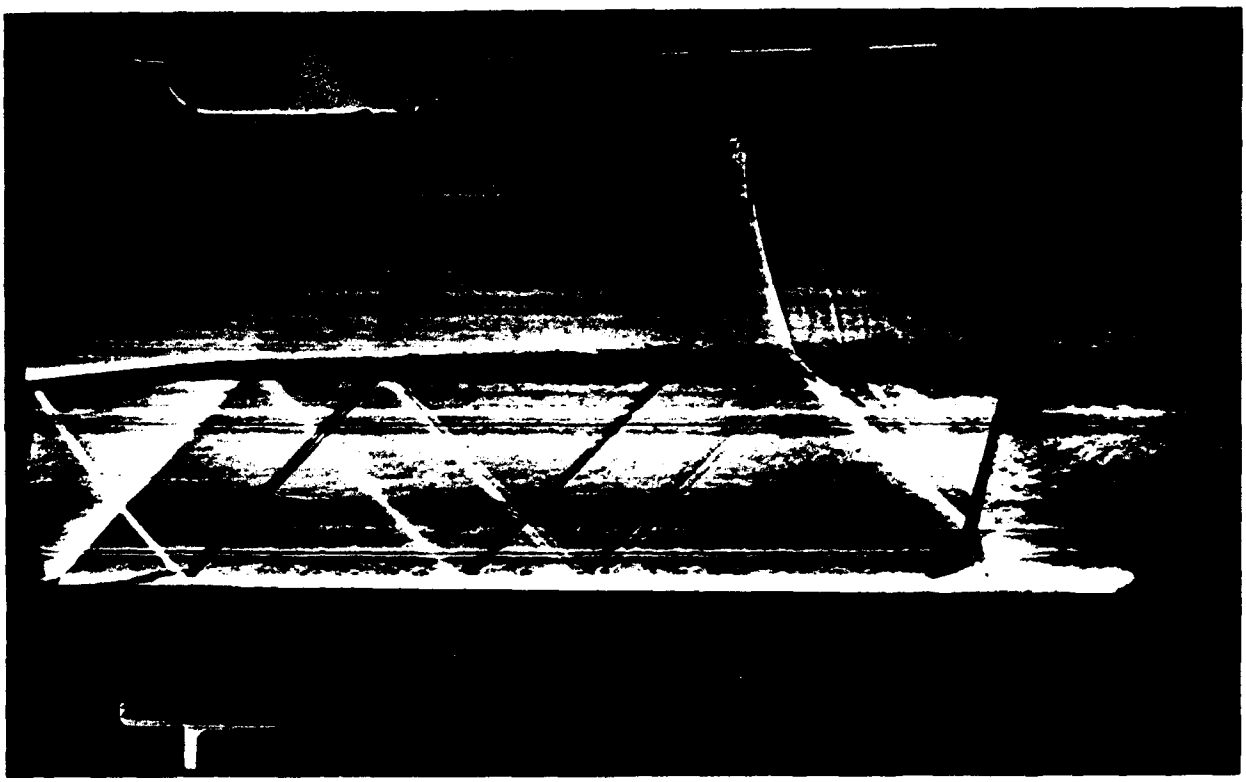

Fig. III.1. Subsonic/supersonic shear layer schlieren-image data. Inlet conditions: $M_1 = 0.65$ [N_2], $M_2 = 1.13$ [N_2]

The first flow condition investigated in the upgraded facility, a $M_1 = 0.65$ [N_2], $M_2 = 1.13$ [N_2] (inlet conditions) shear layer, is shown in the form of a schlieren photograph visualization in III.1. Although this flow is not bi-supersonic at the beginning of the test section (left side of the image), a fan produced by a 5° expansion turn in the lower freestream, on the bottom wall, just upstream of the inlet, curves the shear layer. This results in an aerodynamic Laval nozzle throat, in a manner which causes a Mach number increase in both streams. This produces bi-supersonic

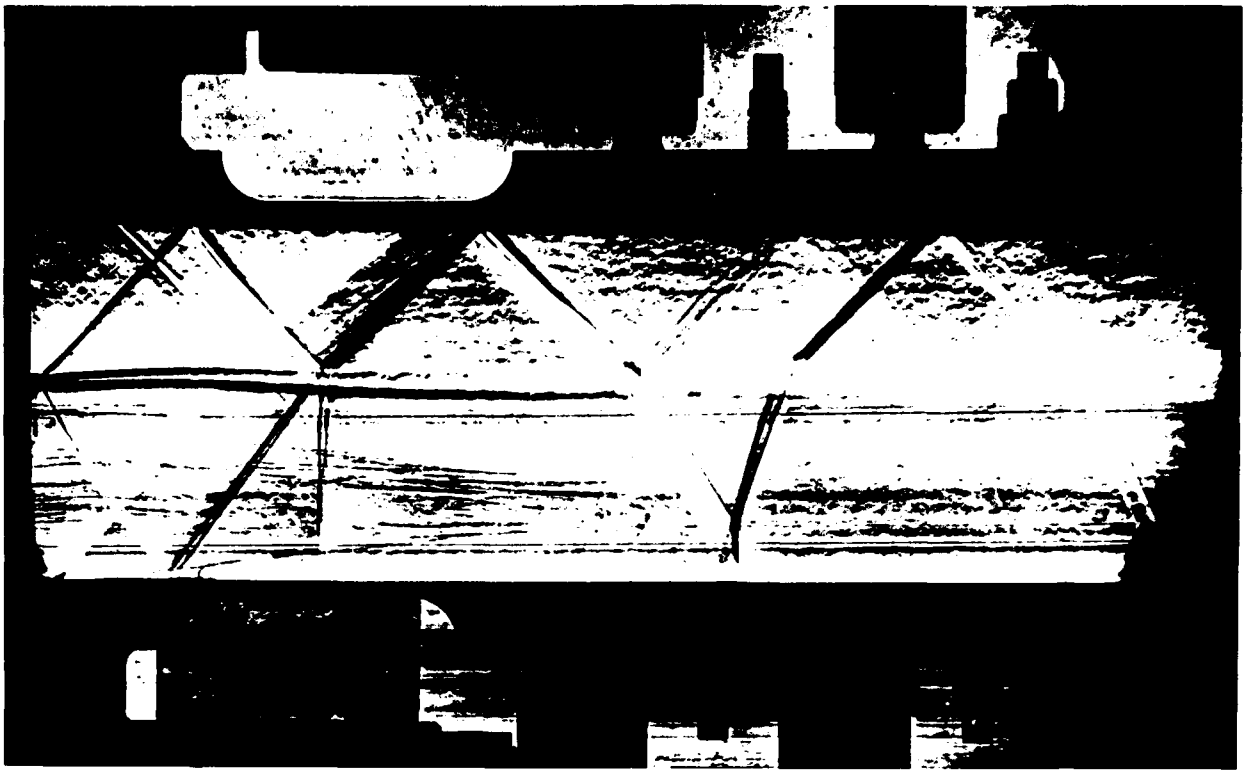

Fig. III.2. Bi-supersonic shear layer schlieren-image data. Inlet conditions: $M_1 = 1.5$ [N_2], $M_2 = 1.13$ [N_2]

flow downstream of the aerodynamic throat, providing an interesting combination of mixed (hyperbolic/elliptic) boundary conditions for this flow configuration.

The first bi-supersonic condition investigated was of a shear-layer flow with inlet conditions $M_1 = 1.50$ [N_2], $M_2 = 1.13$ [N_2]. A schlieren photograph appears in III.2. The most conspicuous difference between this flow, as well as the downstream portion in III.1, and the supersonic/subsonic flows that had been previously investigated in this facility, *i.e.*, supersonic high-speed stream and subsonic low-speed stream (Hall *et al.* 1993), is the transmission of the high-speed stream oblique shock waves into the low-speed stream. Such a transmission of stationary (in the laboratory frame) shocks through the turbulent mixing zone can only occur in a bi-supersonic configuration. This configuration admits rather complex interactions, as evidenced by the four-wave system observed just above the rightmost numeral "4" in the run identification number, "404".

¿From the schlieren photograph, it can be seen that the visual growth rate of the shear layer is not substantially altered by these wave-turbulence interactions. This insensitivity, however, is to be expected, given the weak nature of the incident waves and the near-unity density ratio ($\rho_2/\rho_1 \approx 0.89$) of this flow. Additionally, the shear layer growth rate realized in this experiment is very nearly that of the corresponding, *i.e.*, same velocity and density ratio, incompressible shear layer. In terms of the total convective Mach number,

$$M_c \equiv \frac{U_1 - U_2}{a_1 + a_2} \tag{8}$$

(*e.g.*, Sandham & Reynolds 1989), this result is not surprising; this shear layer should be regarded as incompressible, with $M_c \approx 0.1$.

An additional feature of the wave-turbulence interactions observed in this flow is that shocks refract across the shear layer almost discontinuously. The waves exhibit "kinks" within the shear layer. This indicates that the transverse (vertical in III.2) extent of the Mach number fluctuations is much smaller than that of the density fluctuations, implying considerably different transverse extents (widths) for the Mach number and density profiles. Such behavior was also documented in the incompressible shear-layer investigations by Brown & Roshko (1974). This difference may be of considerable importance in viewing the results obtained by linear stability analyses, for example. The majority of such analyses employ Mach number and density profiles of the same width as inputs to the computations.

This work is part of the Ph.D. research effort of M. Slessor.

III.2 Planar laser Rayleigh-scattering imaging

As part of our effort to investigate compressible, turbulent, shear-layer flows we have continued the development of planar, laser-imaging techniques. In recent experiments, we have extended our previous measurements (Rosemann *et al.* 1992) with improvements in image signal-to-noise ratio. New time-resolved ($\tau \simeq 9\,\mathrm{ns}$), planar, laser-Rayleigh scattering images have been recorded, in non-reacting supersonic shear layers, for convective Mach numbers with respect to the low-speed stream, *i.e.*,

$$M_{c2} \equiv \frac{U_c - U_2}{a_2} \,, \tag{9}$$

in the range of $0.5 \leq M_{c2} \leq 1.5$. The more recent results were presented at the 1993 Annual Meeting of the American Physical Society, Division of Fluid Dynamics (Fourguette *et al.* 1993).

These experiments were conducted in the Supersonic Combustion Facility in flow conditions that had previously been documented. The beam of a frequency-doubled Nd:YAG laser (250 mJ in a 9 ns pulse) was steered through an optical window into the experimental test-section and shaped into a sheet of light. The sheet was passed through slits in the guide walls that acted as "aerodynamic" optical windows and intersected the shear layer such that a vector contained in the image plane was colinear with the flow direction. The Rayleigh-scattered light was collected at right angles to the planar probe region and imaged onto a cryogenically-cooled, 1024 x 1024 pixel, CCD array of a PHOTOMETRICS camera system. The image data were digitized using a 14-bit A/D converter and transferred to a VAX cluster for subsequent storage and processing.

Figures III.3 and III.4 depict examples of such planar-image data. The flows correspond to shear layers with total convective Mach numbers (*cf.* 8) of $M_c = 0.54$ and $M_c = 0.94$, respectively. In these data, the flow is from left to right. The high-speed stream occupies the upper part of the image and the low-speed stream the lower part of the image. The imaged region corresponds to a $3.2 \times 3.2\,\mathrm{cm}^2$ area in the flow, *i.e.*, roughly twice the width of the shear layer at that location (17 cm downstream from the tip of the splitter plate).

In III.3, the high-speed stream fluid is nitrogen. In III.4, the high-speed side stream fluid is helium. In both cases, the low-speed stream fluid is ethylene. The ratio of optical cross-sections (low-speed fluid/high-speed fluid) is 3.79 and 234, for the two images, respectively.

These data provide direct confirmation that compressibility plays an important role in the structure of the shear layer, in general, and the mixing process in particular. Even at relatively low compressibility, *i.e.*, $M_c = 0.54$ (III.3), the mixing layer exhibits a different structure than

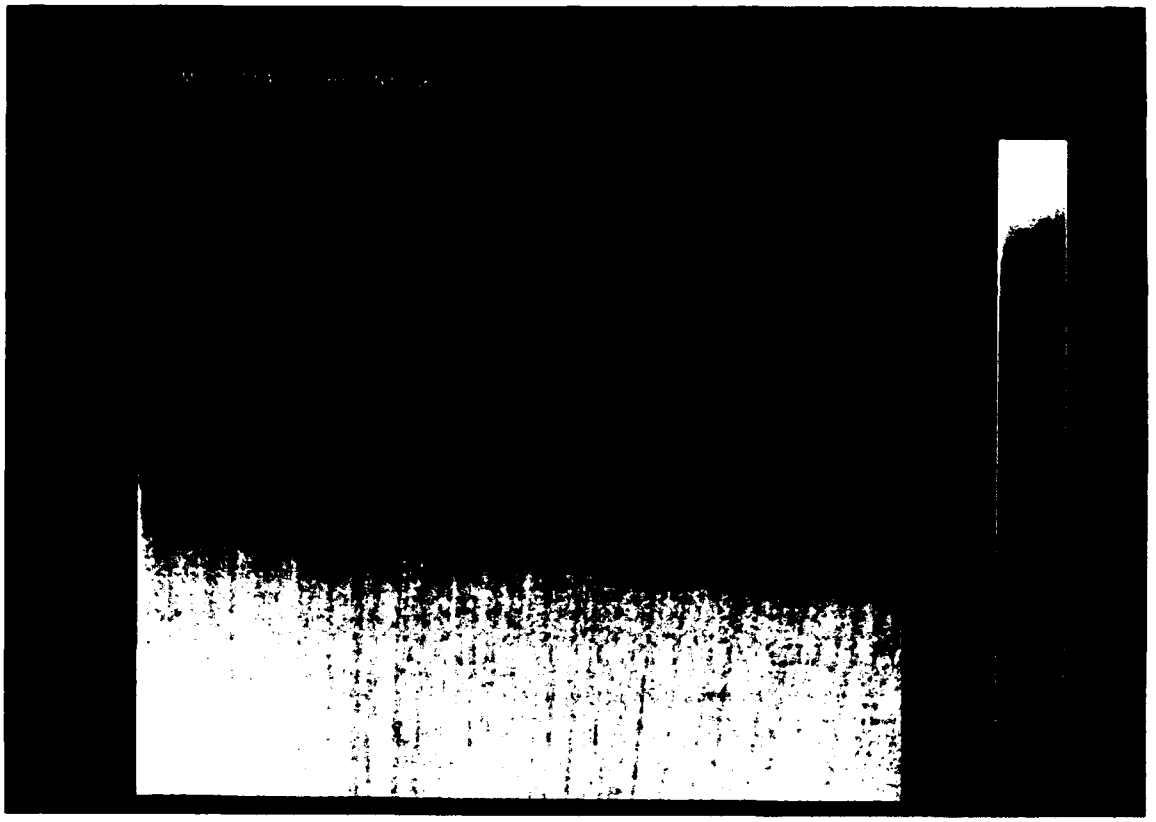

Fig. III.3. Supersonic-subsonic case: $M_c = 0.54$.

the large-scale roller-like structures observed in incompressible shear layers. The low-speed fluid is seen to be peeled off by the high-speed stream. The transport of fluid across the layer appears to occur more through relatively well-defined intrusions of fluid into the opposite stream, rather than through an entrainment process through the rotational motion of organized, large-scale vortical structures. Nevertheless, both these two possibilities are encountered, however, as reflected in local, instantaneous scalar concentration profiles, derived from such images. These show both gradual transitions from high-speed stream fluid to low-speed stream fluid, as was documented by Clemens *et al.* (1991). We also find "plateaus", however, corresponding to regions of well-mixed fluid at an intermediate ratio of high- to low-speed fluid, that are reminiscent of incompressible shear-layer large-scale vortical-structure cores.

In the higher convective Mach number image data in III.4, the structure of the shear layer is different yet from the previous, lower compressibility, case. At these Mach numbers, the low-speed side appears to be shredded by the high-speed stream and regions of uniformly-mixed fluid, encountered in the $M_c = 0.54$ flow, are now not observed. In addition, a wave system can be clearly observed in the low-speed stream. These waves were observed in the same facility using Schlieren imaging (Hall *et al.* 1991, Hall 1991). The signal-to-noise ratio and resolution in these images permits the direct recording of these waves and allows us to conclude that it is the large-scale structures that are responsible for these waves. In particular, this wave system can be seen to be generated by large-scale structures in the shear layer that are convecting with a velocity higher that the speed of sound in the low-speed stream, *i.e.*, an $M_{c2} > 1$. A directly-estimated convective

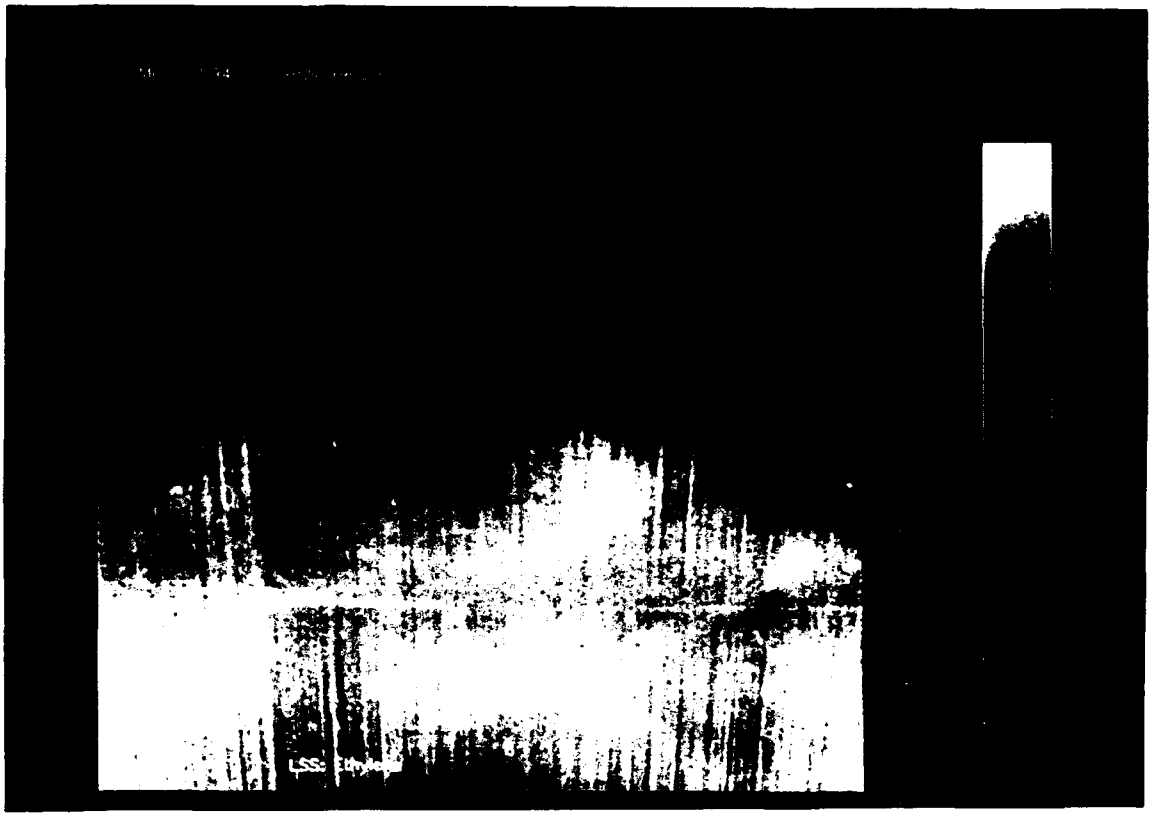

Fig. III.4. Supersonic-subsonic case: $M_c = 0.94$.

Mach number, with respect to the low-speed stream, of $M_{c2} \simeq 2.5$ (9) for this wave can be inferred from the wave angles ($\mu \simeq 24°$) in the low-speed free stream. This estimate compares well with the Hall *et al.* (1991) findings which were based on schlieren data as well as cross-correlation data derived from wall-mounted, high-speed pressure transducers.

This part of the effort is cosponsored by the AFOSR Air-Breathing Propulsion Program, Contract No. F49620-92-J-0290.

III.3 Computation of non-reacting flows

The new multidimensional Godunov scheme (Lappas 1993, Lappas *et al.* 1994a, 1994b) was used to compute a two-dimensional, inviscid, compressible shear layer. The scheme employs the method of Riemann Invariant Manifolds, which can be viewed as the extension of the method of characteristics to the general case of unsteady, multidimensional flow. Computations were performed to compare with recent, high-subsonic/supersonic shear-layer experimental results obtained from the GALCIT supersonic shear layer (S^3L) facility. The parameters for the computations are chosen so that a direct comparison with experimental results is possible.

In all the calculations, a perfect gas is assumed, with constant, specific-heat ratio of $\gamma = 1.4$. The computational domain is the rectangular region: $0 \leq x \leq 2$ and $0 \leq y \leq 1$. The lower boundary, $y = 0$, and upper boundary, $y = 1$, are defined as reflecting walls, and at the right boundary, $x = 2$, outflow boundary conditions are imposed. In particular, the cells at the exit plane, at $x = 2$, are assigned values for the flow invariants identical to those just upstream of the

end cells. The interpolation and integration schemes using the Riemann Invariant Manifolds can then compute the fluid fluxes at the exit plane as if it were an internal interface. This procedure effectively ignores information that may be entering the domain at $x = 2$ from the region $x > 2$. Inflow boundary conditions are specified at the left boundary, $x = 0$, and they are chosen to match the experimental conditions as closely as possible. The splitter plate separates the low-speed (upper) stream, $0.5 < y < 1$, designated by the subscript '1', from the (lower) high-speed stream, $0 < y < 0.5$, designated by the subscript '2'.

Two such runs are presented in the following figures. Mach number contours are given for two cases. In both cases the low speed side corresponds to Mach number $M_1 = 0.65$ and the high speed side to Mach number $M_2 = 1.13$. The high speed stream enters the test section at a 5 degree angle. The first case, shown in III.5, corresponds to an inlet pressure ratio of $p_1/p_2 = 1.05$ and the second case, shown in III.6, corresponds to a pressure ratio of $p_1/p_2 = 1.5$. The initial condition in the entire domain is that of the inflow conditions and the computation is carried out with a CFL number of 0.40 until a steady state is achieved.

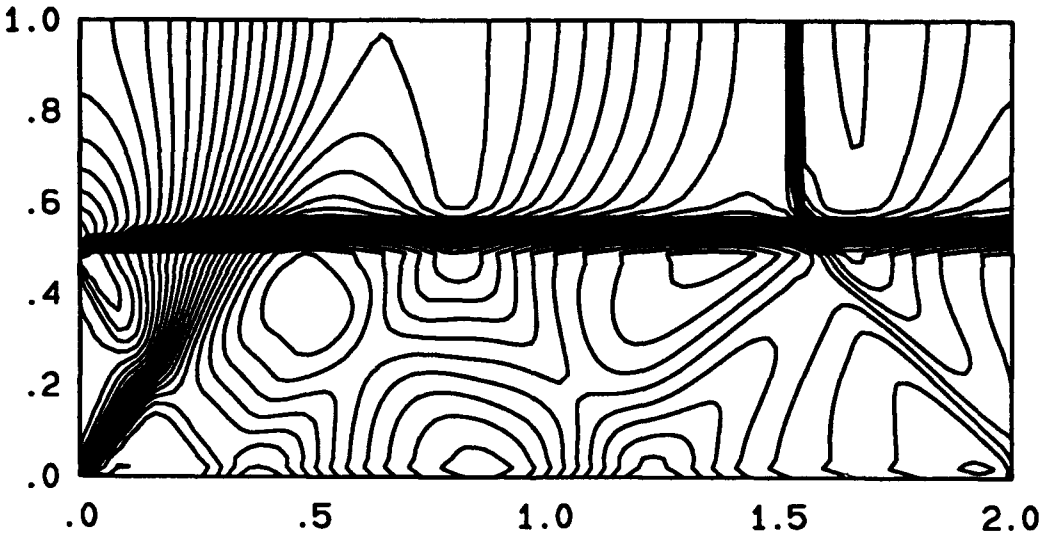

Fig. III.5. Mach number contour levels for a pressure ratio of $p_1/p_2 = 1.05$. There are 60 contour levels in the range $0.6 < M < 1.4$. The resolution is 100×50 cells.

As also found experimentally (*cf.* III.1, III.1), the main feature of the computed flows is that the subsonic low-speed stream is accelerated and becomes supersonic. The shear layer curves and acts as the lower boundary of a gas-dynamic nozzle for the low-speed, initially subsonic, side. In the first case, a normal shock downstream makes the flow subsonic again, whereas in the second case an oblique shock wave system is set up and the low-speed stream remains supersonic through the exit of the computational domain.

III.4 Computation of chemically-reacting flows

As part of our effort to extend these computations to chemically-reacting, compressible, shear-layer flows, we are revisiting the original, Lagrangian, 1-D formulation (Lappas *et al.* 1993), explicitly incorporating finite-rate chemistry in the system equations. At this writing, we have developed

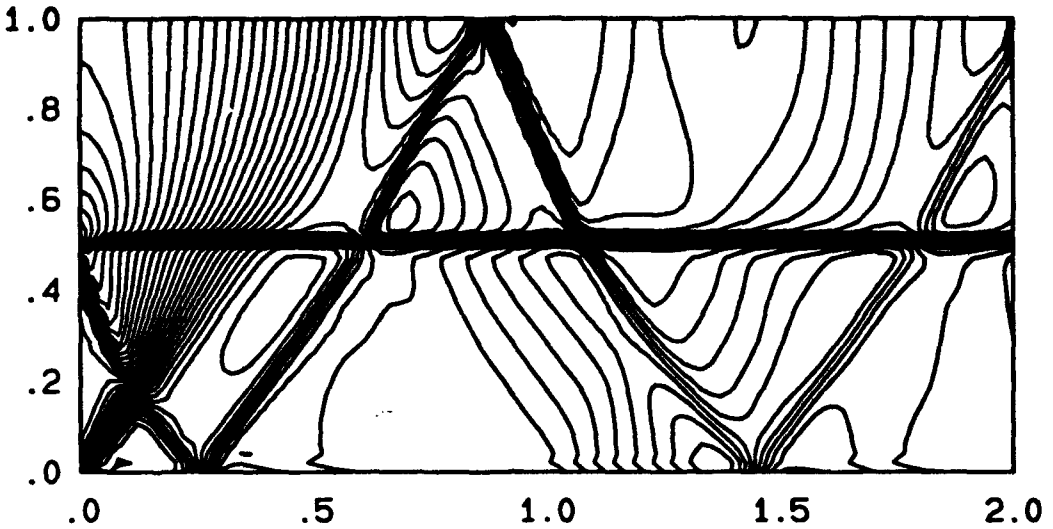

Fig. III.6. Mach number contour levels for pressure ratio $p_1/p_2 = 1.5$. 60 contour levels in the range $0.6 < M < 1.4$. The resolution is 100 x 50 cells.

the algorithm for the computation of 1-D unsteady flows with chemical reactions which treats the fluid mechanics and the chemistry simulteneously in a robust way.

Conventional approaches use the theory of characteristics to develop a number of numerical schemes for integrating this system. In such schemes, the chemical source terms are then integrated separately. in a variety of empirical ways. Usually they are treated in a separate step and considered as a "source" term for the non-reacting flow. The theory of Riemann Invariant Manifolds, developed in the previous stages of this project, however, shows that for multidimensional flow the characteristic surfaces offer no advantage, computational, or otherwise. This is more so the case in reacting flows. Although one can still define characteristic surfaces, they no longer have a simple physical interpretation, because one cannot define a speed of sound in flows where locally there is no chemical equilibrium. Furthermore, the use of conventional methods can not handle the additional problem of the very large range of time and length scales (computational stiffness) associated with chemically-reacting flows.

The new algorithm can be considered as an extention of the theory of Riemann Invariant Manifolds. The key idea is to identify trajectories in spacetime on which appropriate invariants exist for the chemically-reacting case. This allows us to integrate the governing equations in a mathematically consistent way. We expect the first results in the course of the next few months.

This work is part of the Ph.D. research effort of M. Papalexandris.

References

Brown, G. L., and Roshko, A., [1974] "On Density Effects and Large Structure in Turbulent Mixing Layers," *J. Fluid Mech.* **64**, 775–816.

Clemens, N. T., Paul, P. H., Mungal, M. G., and Hanson, R. K., [1991] "Scalar Mixing in the Supersonic Shear Layer," *AIAA 22nd Fluid Dynamics, Plasma Dynamics and Lasers Conference*, AIAA–91–1720.

Fourguette, D. C., Bond, C. L., and Dimotakis, P. E., [1993] "Scalar field measurements in supersonic shear layers," *Bull. Am. Phys. Soc.* **38**(12), 2202.

Hall, J. L., [1991] *An Experimental Investigation of Structure, Mixing and Combustion in Compressible Turbulent Shear Layers*, Ph.D. thesis, California Institute of Technology.

Hall, J. L., Dimotakis, P. E., and Rosemann, H., [1991] "Experiments in non-reacting compressible shear layers," *AIAA* 22nd *Fluid Dynamics, Plasma Dynamics and Lasers Conference*, Paper 91-0629.

Hall, J. L., Dimotakis, P. E., and Rosemann, H., [1993] "Experiments in non-reacting compressible shear layers," *AIAA J.* **31**(12), 2247-2254.

Lappas, T., [1993] *An Adaptive Lagrangian Method for Computing 1-D Reacting Flows and the Theory of Riemann Invariant manifolds for the Compressible Euler Equations*, Ph.D. thesis, California Institute of Technology.

Lappas, T., Leonard, A., and Dimotakis, P. E., [1993] "An Adaptive Lagrangian Method for Computing 1-D Reacting and Non-Reacting Flows," *J. Comp. Phys.* **104**, 361-376.

Lappas, T., Leonard, A., and Dimotakis, P. E., [1994] "Riemann Invariant Manifolds for the Multidimensional Euler Equations. Part I: Theoretical Development," *J. Comp. Phys.* (submitted).

Lappas, T., Leonard, A., and Dimotakis, P. E., [1994] "Riemann Invariant Manifolds for the Multidimensinoal Euler Equations. Part II: A Multidimensional Godunov Scheme," *J. Comp. Phys.* (submitted).

Rosemann, H., Dimotakis, P. E., and Hall, J., [1992] "Flow Visualization in Compressible Turbulent Shear Layers," IUTAM Symposium, *Eddy Structure Identification in Free Turbulent Shear Flows*, 12-14 October 1992 (Poitiers, France).

Sandham, N. D., and Reynolds, W. C., [1989] "A Numerical Investigation of the Compressible Mixing Layer," Stanford Report TF-45.

Personnel associated with the Research

C. L. Bond: Graduate Research Assistant, Aeronautics; Science;

P. E. Dimotakis: Professor, Aeronautics & Applied Physics;

D. C. Fourguette: Post-doctoral Research Fellow, Aeronautics;

D. B. Lang: Aeronautics Staff Engineer;

T. Lappas: Graduate Research Fellow, Aeronautics;

A. Leonard: Professor, Aeronautics;

J. D. Melvin: Member of the Technical Staff, Div. of Engineering & Applied Science;

M. V. Papalexandris: Graduate Research Assistant, Aeronautics;

M. D. Slessor: Graduate Research Assistant, Aeronautics;

P. Svitek: Member of the Aeronautics Technical Staff;

P. T. Tokumaru: Member of the Aeronautics Technical Staff.*

Degrees earned during reporting period

M. D. Slessor, Master of Science, Aeronautics, 1993

Interactions

Presentations

P. E. Dimotakis, "Supersonic turbulent mixing," Lawrence Livermore National Laboratories Seminar, 10 August 1993.

D. C. Fourguette, "Scalar Field Measurements in Supersonic Shear Layers," Caltech Fluid Mechanics Research Conference, 26 October 1993.

P. E. Dimotakis, "Some Issues in Turbulent Mixing and Turbulence," APS Division of Fluid Dynamics Meeting (Albuquerqe, NM), 21 November 1993.

D. C. Fourguette, "Scalar Field Measurements in Supersonic Shear Layers," APS Division of Fluid Dynamics Meeting (Albuquerqe, NM), 21 November 1993.

P. E. Dimotakis, "Some Issues in Turbulent Mixing and Turbulence," Caltech Fluid Mechanics Seminar, 7 January 1994.

P. E. Dimotakis, "Some Issues in Turbulent Mixing and Turbulence," USC ME/Aerospace Seminar, 11 January 1994.

D. C. Fourguette, "Scalar Field Measurements in Supersonic Shear Layers," USC ME/Aerospace Seminar, 2 March 1994.

A. Leonard, "Direct Simulation of Turbulent Flows," ICASE/Langley Research Center Short Course in "Turbulent Modeling and Prediction," (Newport News, VA), 14–18 March 1994.

M. D. Slessor, "Experiments in Bi-Supersonic Shear Layers," Caltech Fluid Mechanics Research Conference, 18 April 1994.

Consultancy

P. E. Dimotakis, Lawrence Livermore National Laboratories, consulting on turbulent mixing, gasdynamics and compressible turbulence.

---

* Through 31 March 1994. Presently, Post-doctoral Research Fellow at the University of Southern California and part-time Member of the Aeronautics Technical Staff.

CHAPTER IV
CHEMISTRY IN NONUNIFORM FLOW

IV.1 DISSOCIATION RATES WITH VIBRATIONAL NONEQUILIBRIUM

Objectives and Status of Research

One of the primary uncertainties in the modeling of hypersonic reacting flows is how the vibrational state of a molecule affects its dissociation rate. Therefore, the main objective of this research is to test chemical reaction rate models in the presence vibrational nonequilibrium. To do this, we are using experimental results from the Caltech T5 shock tunnel to assess the vibration-dissociation coupling models that are used in computational fluid dynamics codes. These models will then be used to design further experiments in T5 to refine our understanding of the effect of vibrational nonequilibrium on reaction rates. These new experiments will determine if the current models are lacking in their ability to predict important flow features. If not, this set of experiments will provide assistance in developing new, more physically consistent models.

To date, all of the currently used vibration-dissociation coupling models have been implemented in a two-dimensional thermo-chemical nonequilibrium computational fluid dynamics method. The models that have been tested are the Park TT_v model, the CVD and CVDV models of Treanor and Marrone, the model of Macheret and Rich, and the model of Olynick and Hassan. The flow of reacting nitrogen over a sphere has been simulated using these models and compared to available experimental data from T5. The shots were made in a high density flow regime where the vibrational nonequilibrium zone is small compared to the entire flow field. Under these conditions, it was found that while the various models gave different vibrational temperature distributions, the shock stand-off distances and density contours are very similar. Thus, these comparisons with previous experiments show that all of the vibration-dissociation models are able to predict the shock stand-off distances and density fields correctly. Fig. IV.1 shows both the experimental interferogram and a computed interferogram for the Park model. The computed shock stand-off distance is accurate to within a tenth of a millimeter, while the fringe patterns are virtually identical.

A new experiment is being designed for T5 that will be more sensitive to the differences in the reaction rate models. Simulations have been made of T5 flows over spheres at lower densities, and differences among the models are discernible in both the shock stand-off distances and the density contours. Fig. IV.2 shows the computed density contours for the Park and the CVDV models at a density of $10^{-5}\,\mathrm{kg/m^3}$. It can be seen that the shapes of the contours in the shoulder region differ dramatically. Future experimental results will be used to determine which of the models, if any, give the correct results.

In addition, computational studies are being carried out to study the effect of the choice of oscillator model and relaxation time expression on the vibration-dissociation coupling problem. Once appropriate test cases have been determined, experimental results will be able to determine which choices yield the best results.

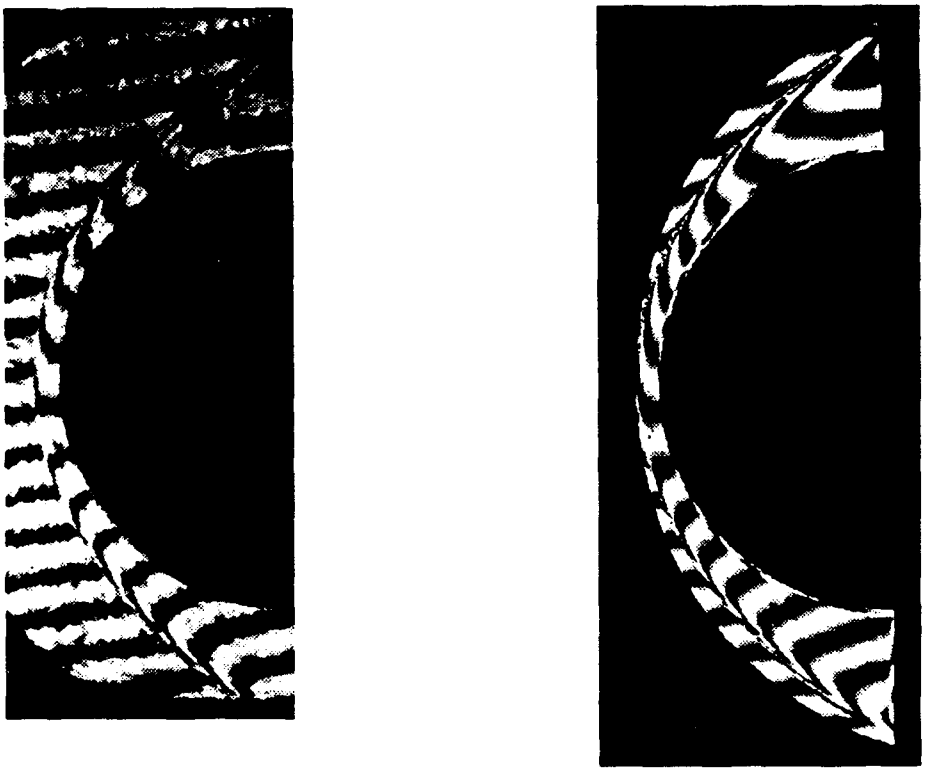

Fig. IV.1. Comparison of experimental (left) and computational (right) differential interferograms of Nitrogen flow over a sphere. Free-stream conditions: $u_\infty = 5070\,\mathrm{m/s}$, $\rho_\infty = 0.0402\,\mathrm{kg/m^3}$, $T_\infty = 2260\,\mathrm{K}$.

References

1. Park, C., "Assessment of Two-Temperature Kinetic Model for Ionizing Air," *AIAA Paper No. 87-1574*, June 1987.

2. Treanor, C.E. and Marrone, P.V., "Effect of Dissociation on the Rate of Vibrational Relaxation," *Physics of Fluids*, Vol. 5, No. 9, pp. 1022-1026, 1962.

3. Marrone, P.V. and Treanor, C.E., "Chemical Relaxation with Preferential Dissociation from Excited Vibrational Levels," *Physics of Fluids*, Vol. 6, No. 9, pp. 1215-1221, 1963.

4. Macheret, S.O. and Rich, J.W., "Theory of Nonequilibrium Dissociation Rates Behind Strong Shock Waves," *AIAA Paper No. 93-2860*, July 1993.

5. Olynick, D. and Hassan, H.A., "A New Two-Temperature Model for Reacting Flows," *AIAA Paper No. 92-2953*, July 1992.

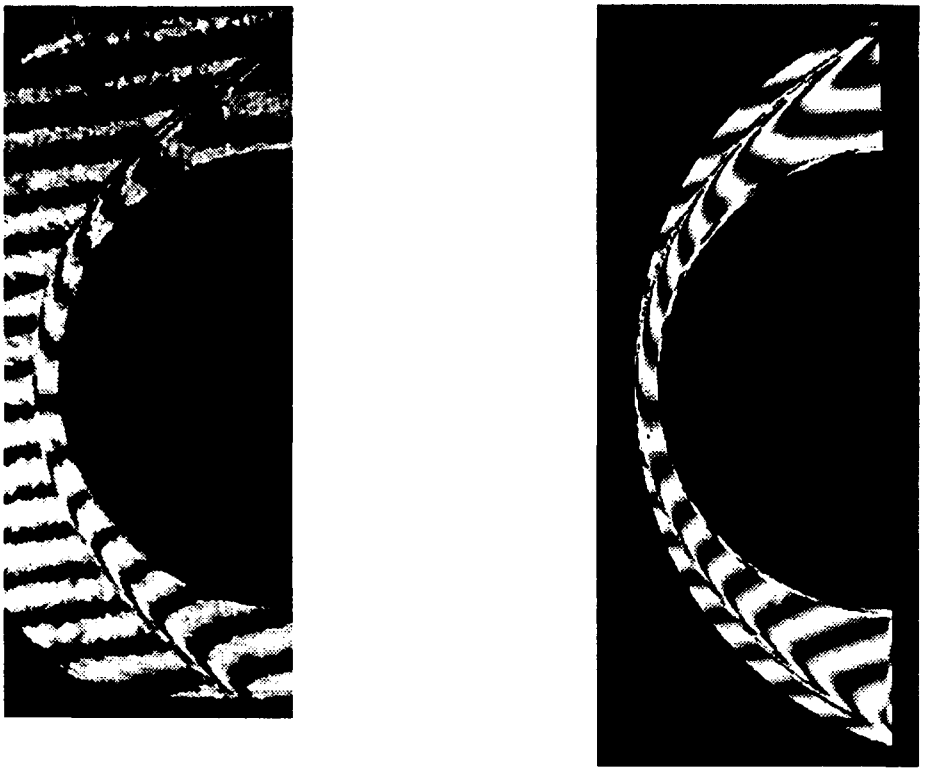

Fig. IV.2. Comparison of the CVDV model (left) and the Park model (right) for the same conditions as those of IV.1 except $\rho_\infty = 0.0402\,\mathrm{kg/m^3}$.

Publications Resulting from Research

Olejniczak, J., G.V. Candler, H.G. Hornung, and C. Wen, "Experimental Evaluation of Vibration-Dissociation Coupling Models," *AIAA Paper No. 94-1983*, June 1994. To be submitted to an appropriate archival journal.

Personnel Associated with Research

Graham V. Candler, Assistant Professor of Aerospace Engineering and Mechanics, University of Minnesota.

Joseph Olejniczak, Graduate Research Assistant, Department of Aerospace Engineering and Mechanics, University of Minnesota.

Interactions

Presentation of research work at the 6th AIAA/ASME Joint Thermophysics and Heat Transfer Conference, Colorado Springs, CO, June 20-23, 1994 (AIAA Paper No. 94-1983).

IV.2 ELECTRON-DRIVEN REACTION RATES IN HYPERSONIC FLOW

Background and Objective

Electrons resulting from ionization due to bow-shock heating play an important role in determining the physical and chemical properties of hypersonic flows.

Processes of interest include vibrational excitation, formation of negative ions (which may then fragment), and electron impact excitation and deexcitation of excited metastable states. Furthermore, with temperatures as high as 10,000 Kelvin due to non-equilibrium overshoots, electrons in the tail of the energy distribution function can lead to electronic excitation of ground state species, particularly those that are vibrationally excited. The available data base for these electron-molecule collision processes which can occur in flowfields is generally fragmentary, and, in many cases, inconsistent. Furthermore, cross sections for electronic excitation of molecules by electrons with barely enough energy to drive the excitation and for electron collisions with electronically excited molecules and with radicals such as OH are essentially *non-existent* and *experimentally inaccessible.* Finally, the experimental effort to measure electron-molecule collision cross sections is very limited and shrinking in the United States.

An obvious strategy for obtaining these electron collision cross sections is to calculate them. However, the significant computational demands of such calculations have made such an approach impractical to date with conventional (sequential) computers. *The objective of our work is to exploit the high-performance computing provided by parallel computers, consisting of arrays of commercially available microprocessors, to calculate the cross sections for electron-molecule collisions needed in modelling the chemical and physical properties of hypervelocity flows.* With appropriate computational strategies, the high aggregate speeds and large memory of these parallel computers make such an approach feasible.

Progress and Highlights

At the relatively low impact energies of interest in hypersonic flowfields, the accurate treatment of the electron-molecule collision process is a computationally challenging problem. In these studies we employ a multichannel extension of the variational principle for scattering amplitudes originally introduced by Schwinger.[1] This formulation, known as the Schwinger multichannel method,[2] was specifically designed to address low-energy electron-molecule collisions.

As in most variational approaches, there are two major computational tasks in these studies: (*i*) calculation of the primitive matrix elements of the operators arising in the variational expression for a given expansion basis, and (*ii*) transformation of these primitive matrix elements to generate the physical matrix elements of the linear equations defining the variational solution. In the Schwinger multichannel method, as in the original Schwinger method, the trial wave function need not satisfy scattering boundary conditions; *square-integrable functions such as Cartesian Gaussians may be employed.* In this basis all matrix elements in the variational expression can be evaluated analytically, except those involving the Green's function. These Green's function matrix elements have no known analytic form and must be done by quadrature. In fact, evaluation of these matrix elements becomes the computationally intensive step of our calculations. The occurrence of these difficult matrix elements in variational principles based on integral equations has discouraged their

use to date, in spite of highly desirable features of these approaches such as the flexibility of employing trial functions which do not satisfy scattering boundary conditions and their very favorable convergence.

Though initially implemented on conventional (sequential) computers, the computationally intensive step of these calculations is ideally suited to computers of distributed-memory parallel architectures. Its most compute-intensive tasks are (*i*) the evaluation of a very large number (typically 10^{10} or more) of elementary integrals describing the interaction of pairs of electrons, a step requiring a code of about 2000 lines of Fortran, and (*ii*) the transformation of these elementary quantities into the matrix elements appearing in the variational expression. The evaluation of the two-electron integrals is readily parallelized: one simply has each processor independently calculate a different subset of the integrals. Step (*ii*), the transformation of the integrals, can be organized as a series of large distributed matrix multiplications between the global array of integrals and a distributed transformation matrix that is easy to construct.

With this strategy for parallelization of our computation, we have achieved sustained performance of about 4 GFLOP on the full Intel Delta, a parallel computer consisting of over 500 i860 microprocessors. This is approximately 100 times the performance of the original sequential program on the CRAY Y-MP. Recently we have successfully ported this parallel code to the CRAY T3D, a multicomputer with 128 DEC alpha processors. On this machine we have achieved performance approximately 50 times that of the CRAY Y-MP.

We have exploited this computational procedure and the parallel computer resources available at the Institute and the Jet Propulsion Laboratory to carry out the following calculations relevant to the modelling of hypersonic flows:

• We have studied the cross sections for near-threshold excitation of the long-lived $A\,^3\sum_u^+$ state of N_2 by electrons. These near-threshold excitation processes are difficult to study experimentally due to the very low post-collision energy of the electron. For this system some limited cross section data based on detection of the metastable state itself is available at about 2 eVs above threshold.[3] Comparison of our calculated cross sections with this data is very encouraging.

• We have completed the first calculation of the cross sections for excitation of the $B^3\Pi_g$ state of N_2 by electron impact on its long-lived $A\,^3\sum_u^+$ state. We believe that such cross sections for electron impact on electronically excited metastable states can play an important role in modelling the chemical and physical properties of hypersonic flows. These cross sections would be generally inaccessible experimentally. Calculations of these cross sections required significant changes in our computer codes and additional calculations of these cross sections are under way.

• We have obtained preliminary results for near-threshold excitation of the lowest excited electronic state ($^3\sum_u^+$) of CO_2.

In summary, we believe that these applications of highly parallel computers to the calculation of electron-molecule collision cross sections are an early indication of the revolutionary impact that parallel computers can be expected to have on our ability to robustly model complex physical and chemical systems.

References

1. J. Schwinger, Phys. Rev. **72**, 742 (1947)

2. K. Takatsuka and V. McKoy, Phys. Rev. A 30, 1734 (1984);

3. C. Winstead and V. McKoy, Phys. Rev. A 5, 648 (1972)

Publication

The results of our calculations of the electron impact excitation cross sections for N_2 and CO_2 outlined above will be prepared for publication within the next six months. We expect these results to lead to two publications.

Personnel associated with the Research

Principal Investigator: Vincent McKoy, Professor of Theoretical Chemistry.

One graduate student (C-H. Lee) and a postdoctoral fellow (H. Pritchard, part-time) are involved in this research effort.

Presentations

The research outlined above has been presented at the following seminars and meetings:

- Colloquium speaker at the Institute for Space and Astronautical Sciences, Tokyo, Japan (July, 1993)

- Colloquium speaker at the Institute for Physical and Chemical Research (RIKEN), Tokyo, Japan (July, 1993)

- Invited speaker at the Gaseous Electronics Conference, Montreal, Canada (October, 1993)

IV.3 NONEQUILIBRIUM LEEWARD SHOCK-VORTEX AERODYNAMICS

Objectives and Status of Research

The objectives of this research are to study the hypervelocity flow at enthalpy sufficient to activate dissociation/recombination chemistry about cones and slender bodies at large incidence, with particular reference to the effect of chemistry on the structure of the leeward flow shock/vortex system. Significant progress has been made in two relevant areas. These are

(1) Completion of the detailed study of the pseudo-Euler flow past a cone at incidence. This is described in detail in a forth-coming publication (Macrossan & Pullin, 1994).

(2) The development and testing of a flexible, viscous, three-dimensional (3D) frozen flow code, *PGP3D*, on the Caltech Intel *Paragon* parallel computer. Detailed testing of this code is described by (Mallett, Macrossan & Pullin, 1994) currently submitted to J. Comp. Phys. while calculation of the frozen inviscid and viscous flow about a blunt nosed delta wing at incidence is given in (Mallett, Pullin & Macrossan, 1994), submitted to the *AIAA J.*.

The next stage of the work, namely the incorporation of the Lighthill-Freeman ideal-dissociating gas chemistry model into *PGP3D* is planned for the near future. A comprehensive statement of significant accomplishments in the areas (1) and (2) above is outlined below. These statements constitute the current status of the research effort. They are followed by a brief statement of the expected progress within the next year.

Personnel associated with the Research

(1) D. I. Pullin, Professor of Aeronautics.

(2) Dr. M.N. Macrossan, University of Queensland, Australia. Collaborator.

(3) Dr. R. Mallett, Postdoctral Fellow 1993. Consultant. Author of principal 3-D inviscid and viscous code.

(4) Mr Shaun Shariff, Postgraduate student. Phd project will probably be the viscous cone flow with reaction chemistry.

IV.3.1 Inviscid Cone Flow with IDG Chemistry

This study was intended as a precursor of the more complicated viscous flows about cones at incidence and about a blunt-nosed delta wing. The computations were performed with the IDG model of reacting Nitrogen about a 15^0 half-angle cone at 30^0 incidence. Flow conditions were $M_\infty = 5.27$ $U_\infty = 6.13$ km/sec. Several runs were done each with different free-stream dissociation fraction α_∞, densityρ_∞, in the range $\rho_\infty = 1 - 10^{-3} kgm^{-3}$ and free-stream enthalpy H_0 in the range $22 - 28\ MJ\ kg^{-1}$, chosen to generate a range of dissociation chemical length scales $L_s = U_\infty/(d\alpha/dt)_s$ where "s" refers to post-windward shock conditions. Each run was performed over a very long cone in order to study the transition from frozen flow, at axial lengths $x << L_s$ where the flow will be nearly frozen (no active chemistry) through chemical nonequilibrium to equilibrium flow for $x >> L_s$.

Detailed analysis of the flow in the windward shock layer and near the leeward shock-vortex

system have been performed and many flow diagnostics, such as the variation following a particle path along a streamline, of the dissociation fraction α, and of the individual dissociation and recombination reaction rates, have been studied, and are reported in detail in Macrossan & Pullin (1994). We select for special comment here several flow features which we plan to investigate in detail for the viscous case. The first is the relative stand-off position of the windward shock from the cone. It was found that the quantity $\Delta_s/x)/(\rho_s/\rho_\infty)$, where ($\Delta_s$ is the standoff distance scaled against distance from the apex x and ρ_s ρ_∞ are the free-stream and post-shock densities respectively), scales well against x/L_s. This scaling is based on that used by Hornung (*J. Fluid Mech.* **53**, 149,1972) in correlating the shock standoff distance for hypervelocity reacting flow over spheres. It gives a good correlation up to $x/L_s \approx 2$ at which point the data for different stagnation enthalpies separate, leading to an approach to the equilibrium limit which depends on H_0. This has been analysed by Wen (Phd thesis, California Institute of Technology, 1994) for flow over spheres. A related analysis for the cone flow should be possible and is planned.

Second, we discuss the dimensions of the leeward vortex, the lateral scale of which was found to vary significantly with the degree of active chemistry. When plotted as A_v/x^2 versus x/L_s where A_v is a measure of the vortex area in a plane normal to the cone axis, good collapse for near frozen flow, and up to $x/L_s \approx 50$ was found, followed by a separation towards the equilibrium limit.

A general conclusion for the inviscid cone flow is that L_s is an important scaling parameter for the effects of chemistry in both the windward and the leeward flow. However as the body length becomes large compared with L_s, this quantity is *not* the dominant parameter. A one-dimesional streamtube model has been used to determine a more appropriate length scale $L_{r,l}$, for the leeward flow, when the equilibrium limit is approached.

IV.3.2 Viscous 3-D Code PGP3D

A code for the computation of 3-D hypersonic flows (*PGP3D*: Parallel General Purpose 3D) has been implemented on the Caltech Intel *Paragon* computer. The code has been written for maximum flexibility. It is structured as a generalized finite volume, explicit time-marching method. *PGP3D* currently contains switches to select either either pseudo-inviscid of viscous laminar flow. The flux-function routines are structured in such a way that any numerical flux function for computing fluxes across cell interfaces can be utilized by incorporating appropriate subroutines. At present two choices are available, either the equilibrium flux method, a kinetic based scheme based on flux-split at the particle distribution function level, or a fast Riemann solver based in part on the Roe algorithm, with provision for a full Godunov treatment of strong shocks. These methods have been tested in detail against standard results for the hypersonic flat-plate boundary layer problem. This work is described in a publication (Mallett, Macrossan & Pullin, 1994) currently submitted to J. Comp. Phys.

Detailed computations have been done of the pseudo-inviscid and viscous flow about a blunt nosed delta wing of 70° sweep, at an angle of attack of 30°. The freestream Mach number was fixed at 8.7. For the laminar viscous flow two Reynolds numbers of $Re = 2.25 \times 10^5$ and 2.25×10^6, with the initial aim of comparing pseudo-inviscid and viscous leeward flow at large Re. This work is described in detail in a publication (Mallett, Pullin & Macrossan, 1994) currently under review by the *AIAA J.*. Fig. refx1 shows a comparison of Mach number contours for the pseudo-inviscid flow and the two viscous flows at a station along the delta-wing. For the inviscid flow, a strong and curved cross-flow shock is apparent on the leeward side, whilst for the viscous flow, the leeward

Fig. IV.3. Contours of Mach number at $x/L = 0.5$. Left; pseudo-inviscid. Middle; $R_e = 2.25 \times 10^6$. Right;$R_e = 2.25 \times 10^6$

shock is merged with a separating shear layer.

Future work

In order to further test *PGP3D*, it is planned in the near future to repeat at least the $Re = 2.25 \times 10^6$ laminar viscous flow calculation using the Fast Riemann solver in place of the EFM numerical flux function, and to make detailed comparisons of the same flow as calculated by the two methods. At the same time the IDG chemistry model will be incorporated into *PGP3D* in order to investigate the effect of chemistry on the windward and leeward flows for both the cone-flow and the delta-wing flow with particular reference to the shock stand-off distance, the heat transfer on the windward body surface, and the structure of the leeward flow. In the longer term it is planned to incorporate a more complex partial equilibrium model of air (Rein, *Phys. Fluids* , A, 4, 873 1992) into *PGP3D*. Shaun Shariff is currently gaining experience with a 2D version of the code *PGP2D* and it is planned that he will move on to the viscous reacting cone flow in 1995.

Publications resulting from project

Macrossan, M.N and Pullin, D.I., A computational investigation of inviscid, hypervelocity flow of a dissociating gas past a cone at incidence. Accepted for publication in *J.F.M.* In Press, 1994.

Mallett, E.R. A numerical study of hypersonic flow over a blunt-nosed delta wing at incidence. Phd Thesis, University of Queensland, Jan 1994.

Mallett, E.R. Macrossan, M.N. and Pullin, D.I., The equilibrium-flux method for the solution of the Navier-Stokes equations for a compressible ideal gas. Submitted to *J. Comp. Phys.*

Mallett, E.R. Pullin, D.I. and Macrossan, M.N., A numerical study of hypersonic leeward flow over a blunt nosed delta wing. Submitted to *AIAA J.*

CHAPTER V
DIAGNOSTICS

V.1 Introduction

Since the major part of the research in this program is experimental, much of our work is also oriented toward development of better diagnostic methods. In some instances the techniques being developed are very closely coupled to particular projects and the progress in their development can be more effectively presented together with the progress in the sub-project in which they are being applied. This is the case for the development of the new thermocouple heat transfer gauges described in section II.2, and the new high-signal-to-noise laser scattering technique described in section III.

In the case of the following section on laser-induced thermal acoustics, the presentation is separated from a specific application, because it needed to be developed as a project in its own right at firs. The method is now maturing, however, and will be applied to the other sub-projects near the end of the next year of this program.

V.2 DIAGNOSTICS WITH LASER-INDUCED THERMAL ACOUSTICS

Objectives and Status of Research

The objectives of the research described in this subsection are to develop laser-induced thermal acoustics (LITA), a nonlinear optical technique for single-shot measurement of gas and flow properties, including species concentration, temperature, transport properties, and velocity, and to apply LITA to hypersonic flows in T5. These objectives are extended from those in the URI proposal as a consequence of favorable developments during LITA research. The feasibility of this technique and the accuracy of an expression derived for the LITA signal (Ref. 1) were verified in a series of experiments on laboratory air. A second series of experiments, currently under construction, will develop LITA concentration and velocity measurements using a small shock tunnel and blow-down supersonic wind tunnel. These experiments are also for preparation and risk-reduction for LITA studies in T5, which are planned for early 1995.

Equipment for LITA studies furnished through URI and Caltech: narrowband dye laser, Cynosure flashlamp-pumped dye laser and modification, high-pressure test section with optical access, high-resolution (< 3 GHz) echelle spectrometer, Princeton Instruments thermo- electrically cooled CCD camera and recording system, Tektronix four-channel 2 GSamples/s digital storage oscilloscope, Wideband amplifed PMT optical detection system, optics and mounts, triggering electronics.

V.2.1 Description of the LITA technique

Over the past year, work on optical diagnostics for T5 has progressed markedly with the development at GALCIT of LITA, a new technique superior in many respects to "conventional" techniques.

In the first series of experiments LITA has provided relatively simple, accurate, single-shot, spatially resolved measurements of sound speed, transport properties, and collisional thermalization rate in laboratory air. Experiments currently under development will apply LITA for single-shot measurement of these properties, as well as the complex gas susceptibility, susceptibility spectra, and the gas velocity. Absolute species concentration and temperature measurements may be extracted from susceptibility spectra. The work on LITA performed at GALCIT has the interest of the wider combustion diagnostic community because

- quantitative signal analysis is simple (cf., LIF, DFWM),
- exhaustive information about probed species is not required (cf., LIF),
- LITA excels in strongly quenching environments (e.g., where collision rates are high, a requirement for fast chemistry; cf., LIF),
- LITA requires only standard lasers and equipment, and
- LITA's capabilities exceed those of other techniques (e.g., single-shot transport-property, absolute concentration, and velocity measurements)
- LITA signals are relatively strong.

LITA is a four-wave mixing (FWM) technique related to coherent anti-Stokes Raman scattering (CARS) and degenerate FWM (DFWM). In FWM techniques, crossed-laser beams form electric-field interference "gratings" in the probed volume. Electric field gratings generate susceptibility (index-of-refraction) gratings via nonlinearities of the probed medium. These gratings scatter light from a third beam into the signal beam. If the intensity of the signal beam can be related to properties of the medium, FWM can be used to measure these properties remotely. The principal difference between the techniques is the type of nonlinearity used to form the susceptibility gratings. CARS and DFWM form gratings by quantum mechanical effects.* These gratings have short lifetimes (< 5 ns at STP), since they are destroyed by molecular collisions. LITA gratings are acoustic: crossed driver lasers generate acoustic pressure and temperature gratings via electrostriction and thermalization, two semi-classical opto-acoustic effects. Acoustic gratings are damped by thermal and viscous diffusion on a much longer time scale (e.g. 1 μs) than quantum mechanical gratings. Longer time scales permit single-shot time resolution of the evolution of the signal which allows sound speed measurement. Furthermore, the formation and lifetime of acoustic gratings are *enhanced* by quenching, which has the opposite effect on quantum-mechanical gratings.

The mathematics of acoustic grating formation is generally far simpler than that of quantum-mechanical gratings. This makes the expression relating experimental LITA signals to gas properties simpler than that of DFWM or CARS. Thus, it was possible to predict the LITA signal with an analytical expression derived previously from the linearized equations of light scattering and hydrodynamics. By fitting the experimental signal to the prediction, sound speeds could be obtained to an accuracy within the uncertainty of independent determinations ($\sim$0.5%). Transport properties obtained this way matched published quantities to within $\sim$30%. A finite-beam-size effect neglected in the predictive analysis limited the accuracies of these measurements. The analysis has since been

---

* Thermal or acoustic gratings often contribute to DFWM signals, especially at high densities. However, the contribution to the signal from these gratings is generally regarded as "interference" with the (desired) signals from the quantum-mechanical gratings. For this reason, the distinction is made that DFWM gratings are purely quantum-mechanical and LITA gratings are purely acoustic, i.e., LITA signals often interfere with DFWM signals.

extended to include this additional effect, the effect of electrostriction, and the effect of finite laser linewidth. Work is under way to publish the extended analysis and automate LITA data reduction. This maturity in signal analysis was not expected until late in the URI program.

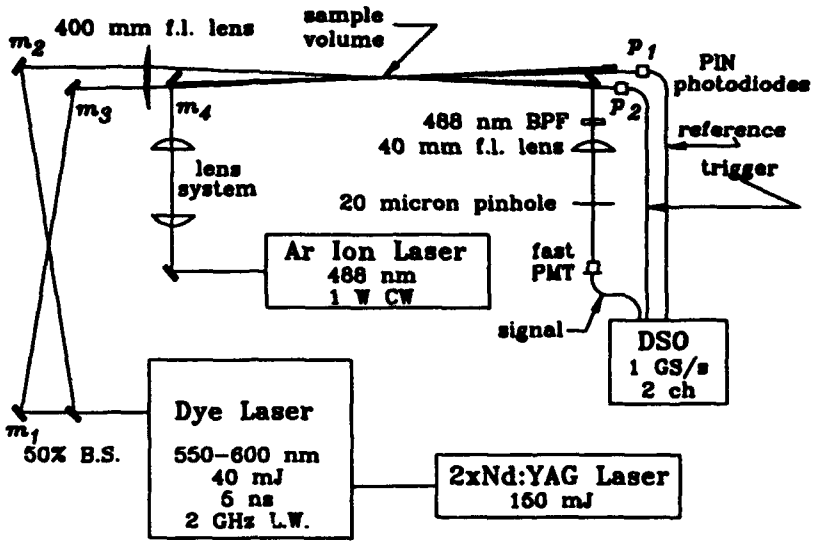

Fig. V.1. Schematic diagram of LITA operation. For notation see text.

V.2.2 Results of demonstration experiments

Experiments conducted to date at GALCIT use the setup schematized in Fig. V.1. A pulsed narrowband dye laser pumped by a Q-switched, frequency-doubled Nd:YAG laser drives the acoustic waves. The dye laser emits about 40 mJ of light tuned between 587 nm and 592 nm in approximately 5 ns pulses. Three-millimeter-wide driver beams are formed from the dye laser emission by a 50% beamsplitter ($B.S.$) and a mirror m_1. The driver beams intersect at the focus of the 400 mm lens where they approximate finite plane waves about 200 μm in diameter. The distance between the parallel beams, adjusted using micrometer translation stages, sets the beam-crossing angle. Three-dimensional phasematching (BOXCARS) geometries with crossing angles ranging from 1.0° to 2.3° were used in these experiments. The acoustic gratings are formed in the sample volume defined by the intersection of these beams. Detection of the driver beam pulse by a silicon PIN photodiode, p_1, triggers the acquisition of the LITA signal. Light from a 1W CW argon ion "source" laser operating at 488 nm scatters coherently off the acoustic gratings into the signal beam. A two-lens system adjusts the source beam diameter, which ranged from about 200 μm to 2 mm. Phasematching adjustments are made using a micrometer-driven translation stage under m_4. A silicon PIN photodiode, p_2, monitors the intensity of the source beam.

The signal beam detection system consists of a fast photomultiplier tube (PMT) with at least a 500 MHz signal bandwidth. Optical filters, including a 10 nm interference filter at 488 nm and a 40 mm lens/20 μm pinhole spatial filter, prevent signal contamination. The LITA signal path-length to the detector is about 2.5 m. Data are recorded using a fast digital storage oscilloscope (DSO). This records typically 500-to-2000-sample time histories of signals from the PMT and p_2.

The first LITA experiments used laboratory air. Nonresonant electrostriction generated LITA signals with a signal-to-source beam intensity ratio, or reflectivity, of $\sim 10^{-8}$. An average over

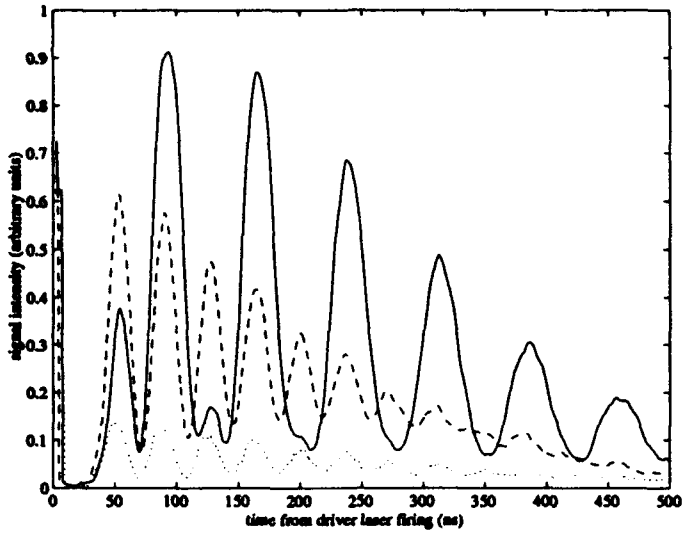

Fig. V.2. LITA signals averaged over 256 shots in room air near a weak line of NO_2. which is present to about 50 ppb. Full line: Signal recorded near the peak of the spectral line. Dashed line: Resonantly enhanced signal near the spectral line. Dotted line: Non-resonant signal. By fitting these to the theoretical prediction, the speed of sound is obtained to $\pm 0.5\%$, and the bulk viscosity to $\pm 10\%$.

256 shots yields the nonresonant data plotted as the dotted curve in Fig. V.2 . The modulation or "ringing" results from beating between Doppler-shifted light scattered off the laser-induced acoustic waves. This occurs at a frequency proportional to the sound speed and known geometrical and optical parameters. The frequency of the modulation (about 26 MHz) yields a sound speed accurate within the uncertainty of the knowledge of the laboratory sound speed ($\sim$0.5%). Electrostriction is resonantly enhanced near absorption lines. The resonantly-enhanced signal recorded near a weak line of NO_2 appears as a dashed curve in Fig. V.2 for comparison. When the driver laser is tuned to an absorption line of the gas, molecules absorb light energy and release thermal energy through inelastic collisions, generating a thermal grating. If thermal gratings form rapidly, expansion of the gas emits acoustic waves. The signal recorded near the peak of the absorption line is the solid curve plotted in Fig. V.2, which shows the difference in signature between electrostriction and thermalization signals. These signals are proportional to the real and imaginary parts of the complex gas susceptibility respectively, allowing measurement of the complex susceptibility. LITA's good sensitivity is demonstrated since the ambient air contained less than 50 ppb of NO_2 according to the Southern California Air Quality Management District.

Seeding the gas with NO_2 provided LITA signals that were several orders of magnitude stronger than the signals obtained from room air, with estimated reflectivities around 10^{-4}. A sample single-shot LITA signal appears in Fig. V.3 with the theoretical fit plotted with a dashed curve, showing excellent agreement with experiment. The sound speed and transport coefficients used in the fit are published values for dry air. Here, the thermalization process is treated as the superposition of two single-rate thermalizations: a fast $\sim$10 ns process and a slow $\sim$100 ns process. A better fit to the data could be obtained by adopting a more accurate thermalization model and source-beam-profile model in the analysis (a top-hat profile is assumed) and including the effect of source-beam phase

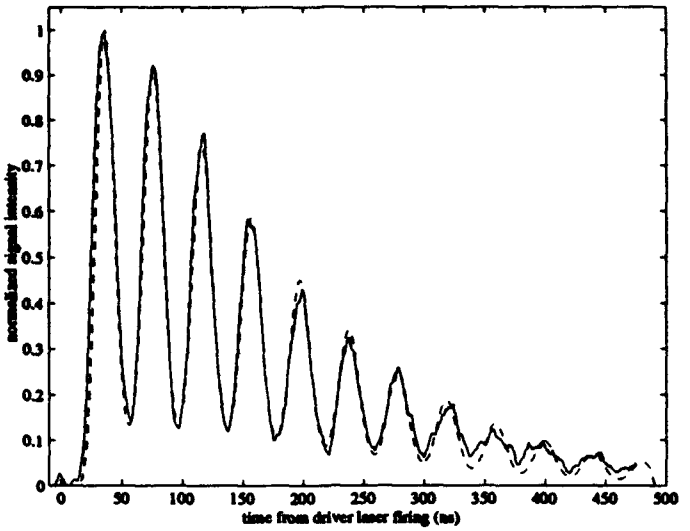

Fig. V.3. Single-shot LITA record in room air seeded with NO_2. Dashed curve shows theoretical prediction.

noise. These improvements are being incorporated into a computer fitting routine for LITA signals.

Information gained from these experiments has guided plans for future experiments. The accuracy of the simple analytical model and the relative strength of LITA signals have opened new paths of exploration: multiplex LITA and LITA velocimetry. Absolute species population and concentration measurements may be extracted from spectra obtained by LITA experiments in which the source laser is scanned across a band of species spectral lines. Such scanning techniques are common in laser diagnostics; however, they are not amenable to pulsed-facilities such as T5. Alternatively, a broadband source laser can be used along with dispersion of the signal beam in a spectrometer to obtain single-shot "multiplex" spectra. Multiplexing using conventional FWM techniques has two drawbacks avoided by LITA.

- Analyzing multiplex spectra from "quantum-mechanical" grating techniques is complicated by quantum interferences, etc. Because LITA uses classical gratings, quantum mechanical complications are avoided. The simple analysis already experimentally verified extends readily to multiplex LITA.
- Much of the energy of the source laser falls between lines and is wasted, thus a high reflectivity is needed. Spectrometer losses compound this effect. LITA signals with reflectivities of 10^{-4} can be used in multiplex experiments studying even trace species. Furthermore, a long-pulse, broadband source laser such as a flashlamp-pumped dye laser may be used. These are available inexpensively with high pulse energies (> 1 J).

Multiplex experiments are currently under construction. A flashlamp-pumped dye laser with about 2.5 J per pulse is being modified for less mode structure. Laser mode structure interferes with all multiplex measurements. A high resolution echelle spectrometer with multiple inputs has been aligned and focused. Spectra fall on a computer-controlled precision CCD array. The spectrometer has a dynamic range of at least 2000:1 and a frequency resolution measured to be better than 3

GHz at 589 nm ($> 10^5$:1).

LITA velocimetry, by analogy with laser Doppler velocimetry (LDV), is also actively being pursued at GALCIT. In this technique, the Doppler shift of light scattered off convecting acoustic gratings is measured relative to an unshifted reference. This should allow single-shot velocimetry in pulsed experiments with flow velocities from 50 to 3000+ m/s (estimation based on detector frequency response, beam size and duration effects etc.) For these experiments, a windowed test section with optical access from four sides has been designed and built. The test section is designed to be used in connection with a variety of test articles including a small combustion-driven shock tunnel capable of generating exit velocities of 3000 m/s in air and 7000 m/s in hydrogen. Alignment and testing will first be performed on a steady ~Mach 2 jet of air from the laboratory air supply.

LITA tests in T5 have been postponed until Spring 1995 to allow experimental development and exploration of the potential for LITA diagnostics. The risk reduction from this measured development and knowledge gained about the use of this promising diagnostic will enhance T5 LITA tests. In addition, timely development of generic LITA capabilities such as spectral multiplexing and velocimetry is in the broad interest of the combustion diagnostic community.

Reference

1. Cummings, E. B. 1992 "Techniques of Single-shot Thermometry by Degenerate Four-wave mixing (DFWM)", GALCIT Fluid Mechanics Report FM 92-2, Caltech, Pasadena, CA.

Personnel associated with the research

1. Hans G. Hornung, Kelly Johnson Professor of Aeronautics, GALCIT Director.
2. Eric B. Cummings, Graduate Research Assistant.
3. Bahram Valiferdowsi, Staff Engineer.

Publications resulting from the reserch

Cummings, E. B. 1992 "Techniques of Single-shot Thermometry by Degenerate Four-wave mixing (DFWM)", GALCIT Fluid Mechanics Report FM 92-2, Caltech, Pasadena, CA.

Cummings, E. B. 1993 "Laser-induced Thermal Acoustics (LITA): Four-wave Mixing Measurement of Sound Speed, Thermal Diffusivity, and Viscosity", Proceedings of the International Conference on Lasers 1993, SOQUE, Mclean, VA.

Cummings, E. B. 1994 "Laser-induced Thermal Acoustics (LITA): Simple, Accurate Single-shot Gas Measurements", 1994 Technical Digest Series, Vol 5, Optical Society of America, Washington, DC.

Cummings, E. B. 1994 "Laser-induced Thermal Acoustics (LITA): Simple Accurate Gas Measurements", to be published in *Optics Letters.*

Cummings, E. B., Hornung, H. G. 1994 "General Expression for Narrowband and "Multiplex" Laser-induced Thermal Acoustic (LITA) Signals" in preparation, to be published in *Applied Optics.*

Interactions

1. Presentation at the International Conference on Lasers 1993, Lake Tahoe, NV, see above.

2. "Laser-induced Acoustics (LIA)" presented at the Gordon Conference on Laser Diagnostics in Combustion, Plymouth, NH.

3. Presentation at the Conference on Laser Applications to Chemical Analysis 1994, Jackson, WY, see above.